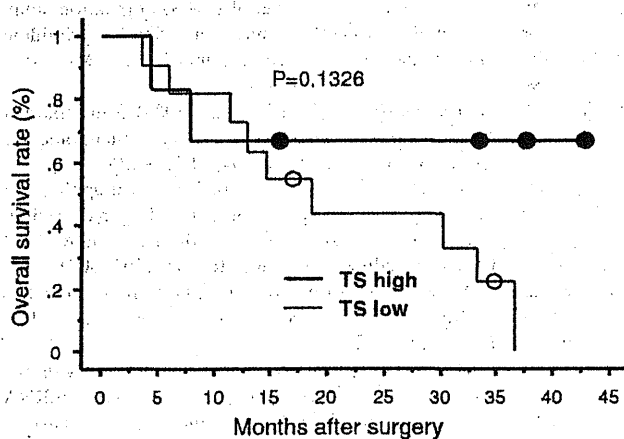**Table 3** Comparison of the backgrounds of the high and low DPD activity groups

	High group (n = 5)	Low group (n = 13)	P value
Age (years)			
Median	64	61	0.51
Range	48–70	52–76	
Sex			
Male	1	9	0.06
Female	4	4	
Histological stage			
III	1	1	0.17
IVa	1	9	
IVb	3	3	
Histological classification			
Well-diff. tub.	2	7	0.10
Mod. diff. tub.	1	4	
Poorly diff. tub.	0	2	
Anaplastic carcinoma	2	0	

Fig. 6 Comparison between the high and the low TS activity groups

measurement of DPD and TS activities in pancreatic cancer by enzyme-linked immunosorbent assay. We showed the clinical significance of DPD and TS activities in pancreatic cancer tissue. The median DPD activity in various solid tumor tissues, including colon, breast, lung and gastric cancer, was reported to be 110.1 pmol/mg protein [21]. We demonstrated that the mean DPD activity in pancreatic cancer tissue was 395.3 pmol/mg protein, and that the DPD activities of all pancreatic cancer specimens were higher than 110.1 pmol/mg protein. Moreover, the DPD activity was upregulated in pancreatic cancer tissues compared with surrounding normal pancreatic tissues in this study. This implies that pancreatic cancer tissue tends to

inactivate 5-FU to a greater degree than surrounding normal pancreatic tissues and other various solid tumors. Therefore, it is necessary to develop an effective 5-FU delivery system and/or 5-FU combined with an inhibitor for DPD that can be used when 5-FU must be administered to patients with pancreatic cancer. Actually, we have already reported that an intra-arterial infusion of 5-FU combined with systemic gemcitabine proved effective for unresectable pancreatic cancer, giving a median survival time of 14 months [22]. Another author reported that a new oral DPD-inhibiting fluoropyrimidine, S-1, is effective against scirrhous gastric carcinoma [23]. Kuramochi et al. used RT-PCR to measure DPD levels in pancreatic cancer patients and found that the DPD expression levels in pancreatic cancer were significantly higher than in other malignancies. They suggested that the high DPD expression level in pancreatic cancer may be a reason for the high effectiveness of S-1 [19]. Our study also indicates that S-1 may be effective, even in pancreatic cancers with high levels of DPD activity. It was also reported that elevated DPD activity may be associated with the malignant potential of bladder cancer [24]. Concerning pancreatic cancer, Miyake et al. showed that patients with a high TP/DPD ratio survived for significantly shorter periods than those with a low TP/DPD ratio. Also, multivariate analysis demonstrated a significantly poorer outcome in patients with a high TP/DPD ratio compared to those with a low TP/DPD ratio. These results support the notion that DPD may be a useful prognostic factor in patients with pancreatic cancer [25]. Those authors found that there was no relationship between DPD mRNA expression and any clinicopathological factors in pancreatic cancer. We also found no such relationship in our study, but there was a tendency for poorly differentiated and anaplastic carcinomas to show high DPD activities.

TS is a critical enzyme in the de novo synthesis of dTMP. dTMP is required for DNA synthesis and is the target for 5-FU. The present study showed that TS activity in pancreatic cancer tissue is significantly higher than that in normal pancreatic tissue, and that the level of TS activity is correlated with the pathological differentiation of pancreatic cancer. The median TS activity in various solid tumors has been reported to be 0.041 pmol/mg protein [18]. In this study, the mean TS activity in pancreatic cancer tissues was 0.028 pmol/mg protein. Therefore, TS activity in pancreatic cancer tissues may be low compared with other solid tumors. High TS expression has been found to be a prognostic factor in colon, gastric, esophageal, breast, and head and neck cancer [26–30], although the role of TS expression in pancreatic cancer is controversial [31, 32]. High TS activity was not associated with poor prognosis in patients with pancreatic cancer in this study.

Histological differentiation is irrelevant to DPD activity. However, anaplastic carcinomas with poor prognosis showed higher TS and DPD activities than the other histological types in this study. This may be one of the reasons why anaplastic carcinoma exhibits resistance to chemotherapy, including 5-FU.

In conclusion, the efficacy of 5-FU may be lower in pancreatic cancer tissue than in normal tissue because DPD activity is upregulated in pancreatic cancer tissue compared to normal pancreatic tissue. DPD-inhibiting fluoropyrimidines such as S-1 may be an effective treatment for patients with pancreatic cancer. Moreover, high DPD activity may be a prognostic factor in patients with pancreatic cancer.

References

1. Silverman DT, Schiffman M, Everhart J et al (1999) Diabetes mellitus, other medical conditions and familial history of cancer as risk factors for pancreatic cancer. Br J Cancer 80:1830–1837
2. Lockhart AC, Rothenberg ML, Berlin JD (2005) Treatment for pancreatic cancer: current therapy and continued progress. Gastroenterology 128:1642–1654
3. Ries L, Harkins D, Krapcho M, Mariotto A, Miller BA, Feuer EJ, Clegg L, Eisner MP, Horner MJ, Howlader N, Hayat M, Hankey BF, Edwards BK (eds) (2006) SEER cancer statistics review, 1975–2003. National Cancer Institute, Bethesda (based on November 2005 SEER data submission, posted to the SEER website; cited 21 Nov 2007)
4. Sener SF, Fremgen A, Menck HR et al (1999) Pancreatic cancer: a report of treatment and survival trends for 100,313 patients diagnosed from 1985–1995, using the National Cancer Database. J Am Coll Surg 189:1–7
5. Sperti C, Pasquali C, Piccoli A et al (1997) Recurrence after resection for ductal adenocarcinoma of the pancreas. World J Surg 21:195–200
6. Griffin JF, Smalley SR, Jewell W et al (1990) Patterns of failure after curative resection of pancreatic carcinoma. Cancer 66:56–61
7. Westerdahl J, Andren-Sandberg A, Ihse I (1993) Recurrence of exocrine pancreatic cancer—local or hepatic? Hepatogastroenterology 40:384–387
8. Beck A, Etienne MC, Cheradame S et al (1994) A role for dihydropyrimidine dehydrogenase and thymidylate synthase in tumour sensitivity to fluorouracil. Eur J Cancer 30A:1517–1522
9. Ota D, Kusama M, Kaise H et al (2004) Evaluation of sensitivity to 5-FU on the basis of thymidylate synthase (TS)/dihydropyrimidine dehydrogenase (DPD) activity and chromosomal analysis in micro tissue specimens of breast cancer. Breast Cancer (Tokyo, Japan) 11:356–366
10. Ichikawa W, Takahashi T, Suto K et al (2004) Thymidylate synthase predictive power is overcome by irinotecan combination therapy with S-1 for gastric cancer. Br J Cancer 91:1245–1250
11. Vallbohmer D, Yang DY, Kuramochi H et al (2007) DPD is a molecular determinant of capecitabine efficacy in colorectal cancer. Int J Oncol 31:413–418
12. Kobayashi H, Koike T, Nakatsuka A et al (2005) Dihydropyrimidine dehydrogenase expression predicts survival outcome and chemosensitivity to 5-fluorouracil in patients with oral squamous cell carcinoma. Oral Oncol 41:38–47

13. Tsuji T, Sawai T, Takeshita H et al (2004) Tumor dihydropyrimidine dehydrogenase expression is a useful marker in adjuvant therapy with oral fluoropyrimidines after curative resection of colorectal cancer. Cancer Chemother Pharmacol 54:531–536
14. Japan Pancreas Society (2003) Classification of pancreatic cancer, 2nd English edn. Kanehara & Co. Ltd., Tokyo, pp 4–12
15. Spears CP, Shahinian AH, Moran RG et al (1982) In vivo kinetics of thymidylate synthetase inhibition of 5-fluorouracil-sensitive and -resistant murine colon adenocarcinomas. Cancer Res 42:450–456
16. Naguib FN, el Kouni MH, Cha S (1985) Enzymes of uracil catabolism in normal and neoplastic human tissues. Cancer Res 45:5405–5412
17. Takechi T, Fujioka A, Matsushima E et al (2002) Enhancement of the antitumour activity of 5-fluorouracil (5-FU) by inhibiting dihydropyrimidine dehydrogenase activity (DPD) using 5-chloro-2, 4-dihydroxypyridine (CDHP) in human tumour cells. Eur J Cancer 38:1271–1277
18. Maring JG, Groen HJ, Wachters FM et al (2005) Genetic factors influencing pyrimidine-antagonist chemotherapy. Pharmacogenomics J 5:226–243
19. Kuramochi H, Hayashi K, Uchida K et al (2008) High intratumoral dihydropyrimidine dehydrogenase mRNA levels in pancreatic cancer associated with a high rate of response to S-1. Cancer Chemother Pharmacol 63:85–89
20. Kamoshida S, Shiogama K, Shimomura R et al (2005) Immunohistochemical demonstration of fluoropyrimidine-metabolizing enzymes in various types of cancer. Oncol Rep 14(5):1223–1230
21. Fukushima M, Morita M, Ikeda K et al (2003) Population study of expression of thymidylate synthase and dihydropyrimidine dehydrogenase in patients with solid tumors. Int J Mol Med 12:839–844
22. Takamori H, Kanemitsu K, Tsuji T et al (2005) 5-fluorouracil intra-arterial infusion combined with systemic gemcitabine for unresectable pancreatic cancer. Pancreas 30:223–226
23. Shimizu T, Yamada Y, Yasui H et al (2005) Clinical application of immunoreactivity of dihydropyrimidine dehydrogenase (DPD) in gastric scirrhous carcinoma treated with S-1, a new DPD inhibitory fluoropyrimidine. Anticancer Res 25:2997–3001
24. Mizutani Y, Wada H, Fukushima M et al (2001) The significance of dihydropyrimidine dehydrogenase (DPD) activity in bladder cancer. Eur J Cancer 37:569–575
25. Miyake K, Imura S, Yoshizumi T et al (2007) Role of thymidine phosphorylase and orotate phosphoribosyltransferase mRNA expression and its ratio to dihydropyrimidine dehydrogenase in the prognosis and clinicopathological features of patients with pancreatic cancer. Int J Clin Oncol 12(2):111–119
26. Edler D, Kressner U, Ragnhammar P et al (2000) Immunohistochemically detected thymidylate synthase in colorectal cancer: an independent prognostic factor of survival. Clin Cancer Res 6:488–492
27. Lenz HJ, Leichman CG, Danenberg KD et al (1996) Thymidylate synthase mRNA level in adenocarcinoma of the stomach: a predictor for primary tumor response and overall survival. J Clin Oncol 14:176–182
28. Harpole DH Jr, Moore MB, Herndon JE 2nd et al (2001) The prognostic value of molecular marker analysis in patients treated with trimodality therapy for esophageal cancer. Clin Cancer Res 7:562–569
29. Romain S, Spyratos F, Descotes F et al (2000) Prognostic of DNA-synthesizing enzyme activities (thymidine kinase and thymidylate synthase) in 908 T1–T2, N0–N1, M0 breast cancers: a retrospective multicenter study. Int J Cancer 87:860–868
30. Harada K, Kawashima Y, Yoshida H et al (2006) Thymidylate synthase expression in oral squamous cell carcinoma predicts response to S-1. Oncol Rep 15:1417–1423

31. Hu YC, Komorowski RA, Graewin S et al (2003) Thymidylate synthase expression predicts the response to 5-fluorouracil-based adjuvant therapy in pancreatic cancer. Clin Cancer Res 9:4165–4171

32. Formentini A, Sander S, Denzer S et al (2007) Thymidylate synthase expression in resectable and unresectable pancreatic cancer: role as predictive or prognostic marker? Int J Colorectal Dis 22:49–55

Signaling and Regulation

**Molecular
Cancer
Research**

Nitric Oxide Inhibits the Proliferation and Invasion of Pancreatic Cancer Cells through Degradation of Insulin Receptor Substrate-1 Protein

Hiroki Sugita[1], Masao Kaneki[2], Satoshi Furuhashi[1], Masahiko Hirota[1], Hiroshi Takamori[1], and Hideo Baba[1]

Abstract

Nitric oxide (NO), which plays a role in the posttranslational modification of proteins, exhibits tumoricidal activity. However, the mechanism remains largely unclear. We investigated whether the regulation of insulin receptor substrate (IRS)-1 protein expression and insulin/insulin-like growth factor (IGF) signaling by NO is involved in the proliferation and invasion of pancreatic cancer cells. NO donor inhibited insulin/IGF-I-stimulated phosphorylation of insulin receptor/IGF-I receptor, IRS-1, Akt/PKB, and glycogen synthase kinase-3β along with decreased expression of IRS-1 protein in MIAPaCa-2 cells, whereas NO donor enhanced the phosphorylation of extracellular signal-regulated kinase-1/2. In contrast, a selective inducible nitric oxide synthase inhibitor, 1400W, upregulated the expression of IRS-1 protein and the phosphorylation of IRS-1, Akt/PKB,-and glycogen synthase kinase-3β, along with enhanced proliferation and invasion of Panc-1 cells expressing inducible nitric oxide synthase protein. NO donor induced IRS-1 protein reduction through increased ubiquitination and degradation. For the detection of the site responsible for NO-induced ubiquitination, IRS-1 deletion mutant genes were transfected and overexpressed in MIAPaCa-2 cells. The results indicate that the COOH terminus of the IRS-1 protein is required for NO donor–induced ubiquitination and protein degradation. Cells stably transfected with COOH-terminal deletion mutants of IRS-1 exhibited reduced IGF signaling and cell proliferation compared with vector alone–transfected cells, with no influence of NO on IGF signaling and invasion, although stable transfectants with full-length IRS-1 protein exhibited remarkable NO-induced reduction in IGF signaling, cell proliferation, and invasion. These findings indicate that NO inhibits the proliferation and invasion of pancreatic cancer cells, at least in part, through upregulation of IRS-1 protein degradation and resultant downregulation of the insulin/IGF-I-Akt pathway. *Mol Cancer Res; 8(8); 1152–63.* ©2010 AACR.

Introduction

Insulin/insulin-like growth factor (IGF) signals play a key role in cancer proliferation and invasion (1-3). Insulin/IGF-I and IGF-II bind to insulin/IGF-I receptors and then phosphorylate the tyrosine of the cognate receptors. Insulin receptor substrate (IRS)-1, an adaptor protein, exists mainly in the cytosol and binds to phosphorylated insulin receptor and IGF-I receptor (IGF-IR), resulting in the phosphorylation and activation of IRS-1. IRS-1 trans-

Authors' Affiliations: [1]Department of Gastroenterological Surgery, Graduate School of Medical Sciences, Kumamoto University, Kumamoto, Japan and [2]Department of Anesthesia and Critical Care, Massachusetts General Hospital, Shriners Hospitals for Children, Harvard Medical School, Boston, Massachusetts

Corresponding Author: Hiroki Sugita, Department of Gastroenterological Surgery, Graduate School of Medical Sciences, Kumamoto University, 1-1-1 Honjo, Kumamoto 860-8556, Japan. Phone: 81-96-373-5212; Fax: 81-96-371-4378. E-mail: sugitaf@ba2.so-net.ne.jp

duces phosphatidylinositol-3 kinase (PI3K), which in turn activates further downstream components, including Akt/PKB and glycogen synthase kinase-3β (GSK-3β). Alternatively, phosphorylated and activated IRS-1 can also bind to another adaptor protein, Grb-2, which activates mitogen-activated protein kinase, another major insulin/IGF signaling cascade parallel to the PI3K-Akt/PKB pathway (4, 5). IRS-1 protein expression was detected in several types of cancer, including pancreatic cancer, breast cancer, and hepatic cell carcinoma (6, 7). Thus, insulin/IGF signal has been considered to play a major role not only in metabolic actions, including stimulation of glucose uptake and synthesis of glycogen and protein, but also in cancer viability including proliferation and invasion. IRS-1 is a key molecule in insulin/IGF signaling, which transduces a signal from the insulin receptor/IGF-IR to the PI3K and mitogen-activated protein kinase pathways (8). However, the mechanism of the regulation of IRS-1 expression and insulin/IGF signals in cancer cells remains unclear.

Recent studies have shown that nitric oxide (NO) plays a role in the posttranslational modification of proteins (9-12). NO is produced by three distinct genes: neuronal and endothelial nitric oxide synthases (nNOS and eNOS) and

inducible nitric oxide synthases (iNOS; refs. 13, 14). In contrast to the activities of nNOS and eNOS that are tightly regulated by calcium-dependent calmodulin binding, iNOS does not require calcium ion or posttranslational modification for its activity. Therefore, iNOS expression is associated with prolonged, exaggerated NO generation up to > 1,000-fold compared with nNOS and eNOS (15, 16). Although iNOS expression is increased in macrophages and endothelial cells by various stimuli, including acute inflammation, recent studies revealed that iNOS is expressed even in normal conditions in many tissues, including skeletal muscle and cancer (17, 18). In the skeletal muscle of diabetic mice, NO was found to play a key role for insulin resistance (17, 19). Controversial results have been reported about the roles of NO in cancer. Recent articles reported that endogenous NO promotes oncogenesis and angiogenesis in various cancers (20, 21). In contrast, other studies have shown that NO inhibits cell proliferation and induces apoptosis in various cells including cancer cells, in vitro and in vivo (22-28). These studies suggest that NO can act either as a tumor suppressor or as a tumor enhancer depending on cell type and the level of NO in the cells. However, the molecular mechanism underlying the inhibitory effects of NO on cancer viability remains unclear.

In this study, we show that NO induces proteasome-dependent IRS-1 protein degradation, and that the regulation of IRS-1 expression and insulin/IGF signaling by NO is involved in NO donor–mediated inhibition of the proliferative and invasive activities of pancreatic cancer cells. These data provide new insight into the molecular basis underlying the regulation of cancer viability by NO.

Materials and Methods

Materials

MG132, S-nitrosoglutathione (GSNO), S-nitroso-N-acetylpenicillamine (SNAP), and L-NAME were purchased from Calbiochem. A highly selective NO inhibitor, 1400W, was purchased from Cayman Chemical. Recombinant IGF-I was purchased from Peprotech. Insulin and anti-Flag antibody were purchased from Sigma. Anti–phospho-Tyr$^{1135/1136}$ IGF-IRβ, anti–phospho-Ser^{473} Akt/PKB, anti–phospho-Ser^9 GSK-3β, anti–phospho-extracellular signal-regulated kinase (Erk)-1/2, anti–Akt/PKB, anti–GSK-3β, and anti–Erk-1/2 antibodies were purchased from Cell Signaling Technology. Anti–IRS-1 antibody was purchased from Upstate Biotechnology. Anti-phosphotyrosine and anti-ubiquitin antibodies were purchased from Santa Cruz Biotechnology. Anti-iNOS antibody was purchased from Becton Dickinson. Geneticin (G-418) was purchased from Life Technologies, Inc.

Cell culture

MIAPaCa-2, Panc-1, MCF-7, MB 468, and HepG2 cells were obtained from the American Type Culture Collection and were maintained in DMEM supplemented with 10% fetal bovine serum (FBS) at 37°C under a humidified atmosphere of 5% CO_2.

Nitrite assay

The concentration of nitrite was determined using a 2,3-diaminonaphthalene kit (Dojindo Laboratories; ref. 29). Briefly, MIAPaCa-2 cells and Panc-1 cells were incubated in phenol red–free DMEM. The medium was centrifuged at 1,000 × g for 15 minutes and the supernatant was placed on 96-well microplates. 2,3-Diaminonaphthalene was added to each well and incubated at room temperature for 15 minutes, and then stop solution was added. The fluorescence intensity of each well at 450 nm (excitation 360 nm) was measured with a fluorescence microplate reader. The concentrations of nitrite were calculated by reference to a standard curve of nitrite.

Constructs

cDNA construct of full-length human IRS-1 (hIRS) wild-type (WT) was produced by reverse transcription-PCR. ssDNA was used as a template, which was produced by reverse transcription using oligo-dT primer from mRNA isolated from HepG2 cells, and then PCR of the single-stranded hIRS-1 WT DNA was performed. For the cDNA construct of the full-length hIRS-1 WT gene, the sense primer was 5'-ATGGCGAGCCCTCCG-GAGAGCGAT-3' and the antisense primer was 5'-CTGACGGTCCTCTGGCTGCTTCTGGAAAC-3'. The PCR was begun with denaturation at 94°C for 5 minutes followed by 35 cycles of denaturation at 94°C for 45 seconds, annealing at 60°C for 1 minute, and extension at 72°C each for 3 minutes 30 seconds with a final extension at 72°C for 10 minutes. AccuPrime Pfx (Invitrogen) was used as the DNA polymerase.

For the production of deletion mutants (DM), PCR was performed using full-length hIRS-1 as a template. The primers used were as follows: DM1, 5'-ATGGC-GAGCCCTCCGGAGAGCGAT-3' (sense) and 5'-GTCCCCCACTGGTGACATGTTCA-3' (antisense); DM2, 5'-ATGGCGAGCCCTCCGGAGAGCGAT-3' (sense) and 5'-CTCATCACTCATGGCCCGCATGGC-3' (antisense); and DM3, 5'-ATGTCCAACAC-CAGCAGCCCCTCCGACTG-3' (sense) and 5'-CTGACGGTCCTCTGGCTGCTTCTGGAAAC-3' (antisense). The PCR was begun with denaturation at 94°C for 5 minutes followed by 30 cycles of denaturation at 94°C for 45 seconds, annealing at 60°C for 1 minute, and extension at 72°C each for 3 minutes with a final extension at 72°C for 10 minutes. AccuPrime Pfx (Invitrogen) was used as the DNA polymerase.

All PCR products were treated with Taq DNA polymerase and then subcloned into pCR2.1-TOPO vector (Invitrogen). Subcloned pCR2.1-TOPO vector was digested by EcoRI and then genes were inserted into pCMV Tag 4A vector (Stratagene), which is a mammalian expression vector, and then treated with EcoRI and CIAP. An illustration of the PCR products of full-length IRS-1, DM1, DM2, and DM3 is provided (see Fig. 2C).
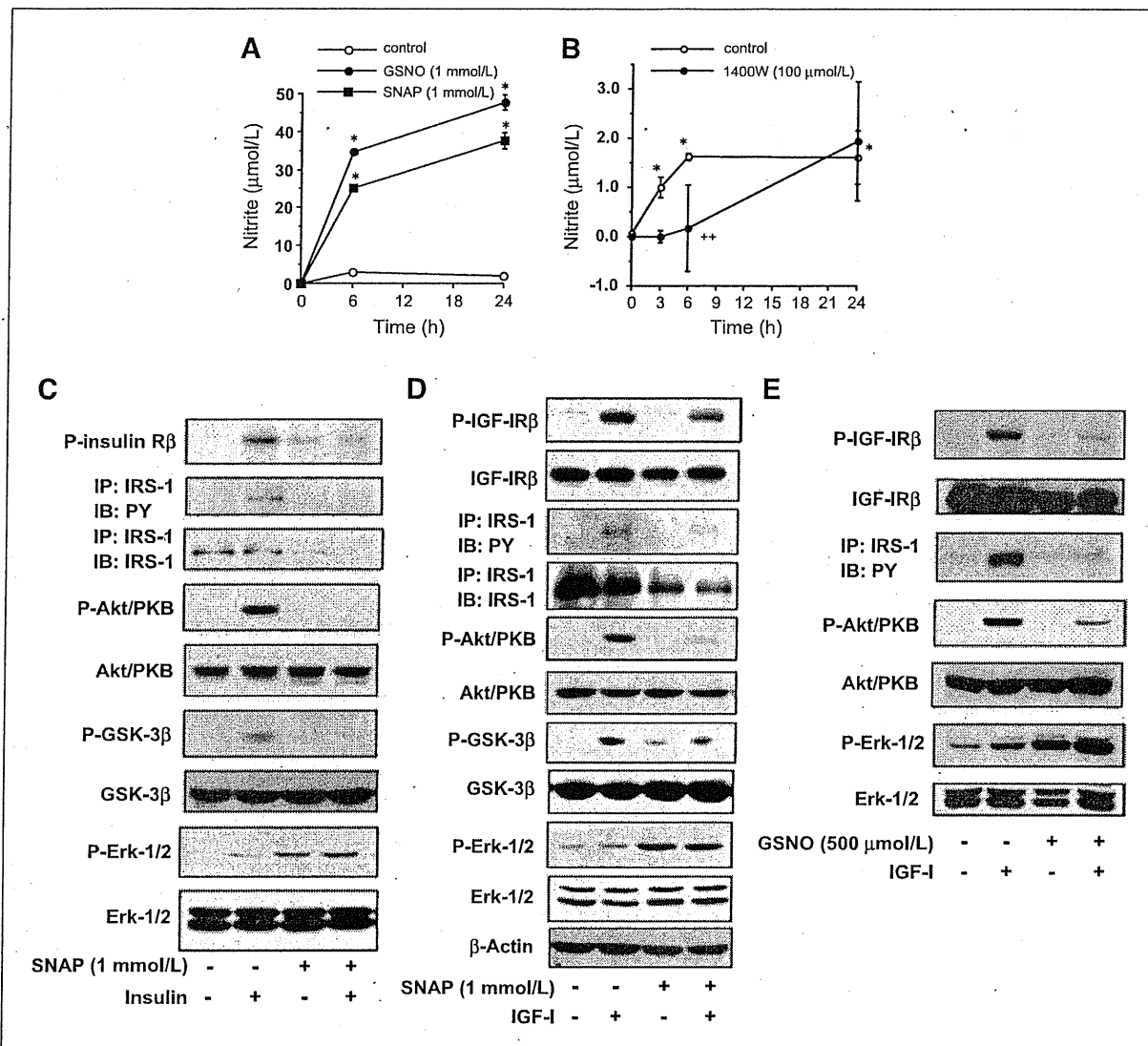
FIGURE 1. A and B, concentration of nitrite in medium. A, MIAPaCa-2 cells were cultured with GSNO (1 mmol/L) or SNAP (1 mmol/L) for 0, 6, and 24 h. The concentration of nitrite in supernatant was determined. *, $P < 0.05$, compared with control. B, Panc-1 cells were cultured with 1400W (100 μmol/L) for 0, 3, 6, and 24 h. The concentration of nitrite in supernatant was determined. *, $P < 0.05$, compared with 0 h. ++, $P < 0.05$, compared with control. C to E, regulation of insulin/IGF signal by NO donor in MIAPaCa-2 cells. MIAPaCa-2 cells, which were incubated in DMEM with 10% FBS overnight and grown to 80% confluence, were used. After incubation with SNAP (1 mmol/L) or GSNO (500 μmol/L) under serum starvation for 6 h, the cells were incubated with insulin (100 nmol/L) or IGF-I (25 nmol/L) for 5 min and then harvested. Cell lysates were subjected to immunoprecipitation (IP) associated with immunoblotting (IB) or immunoblotting. All experiments were repeated three times and the same results were obtained.

Cell transfection

MIAPaCa-2 cells were transfected with pCMV Tag 4A/IRS-1 (full-length), pCMV Tag 4A/IRS-1 DM1, pCMV Tag 4A/IRS-1 DM2 (as a dominant negative), pCMV Tag 4A/IRS-1 DM3, and pCMV Tag 4A vector alone using Lipofectamine 2000 (Invitrogen). Twenty-four hours after transfection, the cells were used for the assay of IRS-1 protein degradation and detection of ubiquitination. In addition, the cells transfected with
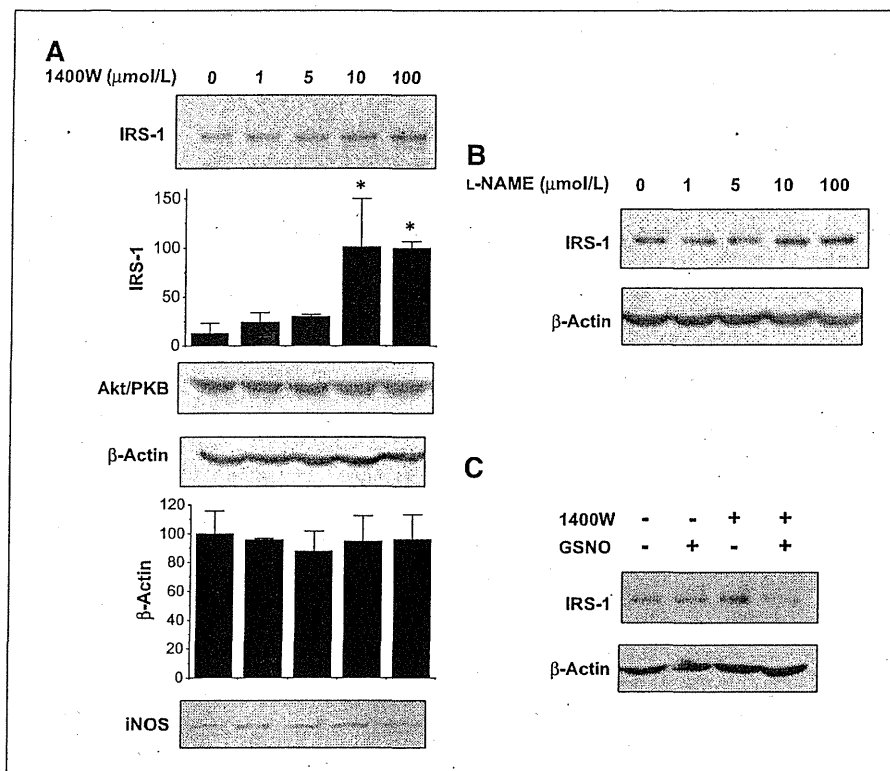
protein expression vectors were incubated with G418 for the selection of transfected gene–expressing cells for 2 weeks and then cloned. The clone that highly expresses the transfected gene was selected and then used for the assays.

Cell lysis

Cell lysates were obtained as previously described (19). Briefly, cells were lysed with cell lysis buffer [50 mmol/L
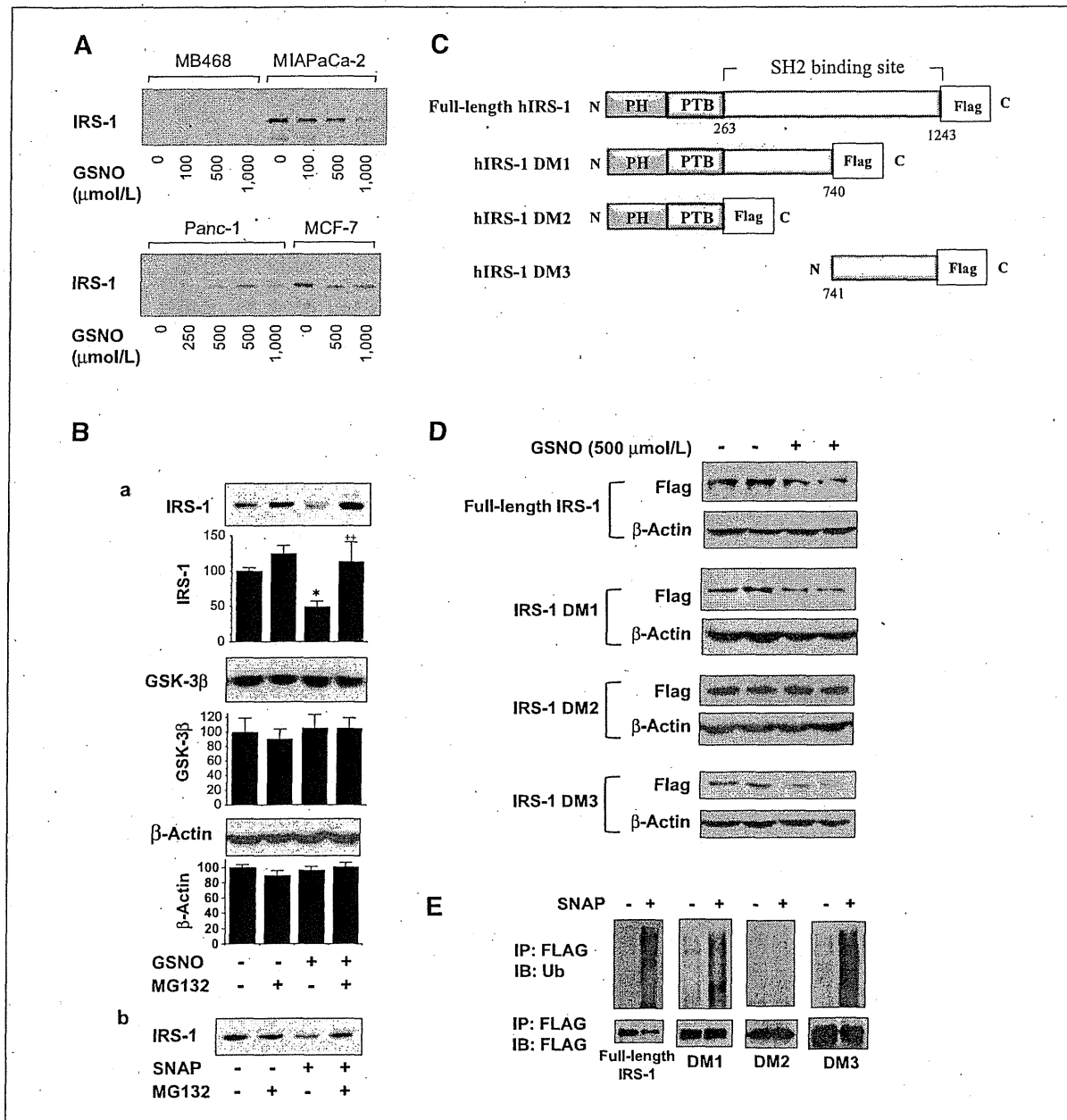
FIGURE 2. NO donor–induced reduction of IRS-1 protein expression through proteasome-mediated degradation in MIAPaCa-2 cells. A, MB 468, MIAPaCa-2, Panc-1, and MCF-7 cells were incubated under various concentrations of GSNO in DMEM with 10% FBS for 24 h. After incubation, cells were harvested and cell lysates were subjected to immunoblotting for detection of IRS-1 protein expression. All experiments were repeated three times and the same results were obtained. B, MIAPaCa-2 cells were incubated in DMEM with 10% FBS overnight. Subsequently, MG132 (3.3 μmol/L), a proteasome inhibitor, was added 30 min before (a) GSNO (500 μmol/L) or (b) SNAP (1 mmol/L) administration, followed by incubation for 24 h. Cell lysates were subjected to immunoblotting for detection of IRS-1 protein expression. Data shown are the results of triplicate experiments. Bars, SEM. *, $P < 0.05$, compared with control; ++, $P < 0.05$, compared with GSNO only. C, schematic representation of the functional domains of hIRS-1 protein and the structural organization of the deletion mutants. PH and PTB indicate pleckstrin homology and phosphotyrosine binding regions, respectively. The various hIRS-1 deletion mutants contain a FLAG epitope (DYKDDDDK) at the COOH terminus. D, MIAPaCa-2 cells were transfected with full-length IRS-1, IRS-1 DM1, IRS-1 DM2, and IRS-1 DM3 using Lipofectamine 2000, followed by incubation with GSNO (500 μmol/L) for 24 h. Each overexpressed protein was detected by immunoblotting using anti-Flag antibody. E, MIAPaCa-2 cells were transfected with full-length IRS-1, IRS-1 DM1, IRS-1 DM2, and IRS-1 DM3. MIAPaCa-2 cells were incubated in DMEM with 10% FBS overnight, and then MG132 (3.3 μmol/L), a proteasome inhibitor, was added 30 min before SNAP (1 mmol/L) administration, followed by incubation for 4 h. For the detection of ubiquitination, cell lysates were subjected to immunoprecipitation with anti-Flag antibody, followed by immunoblotting with anti-ubiquitin. All experiments were repeated three times and the same results were obtained.

FIGURE 3. 1400W, a highly selective iNOS inhibitor, upregulates IRS-1 protein expression and insulin/IGF signal in Panc-1 cells, which express iNOS protein. A, Panc-1 cells were incubated with various concentrations of 1400W for 24 h. Cell lysates were subjected to immunoblotting for the detection of expression of several proteins. Data shown are the results of triplicate of experiments. Bars, SEM. *, $P < 0.05$, compared with control. B, Panc-1 cells were incubated with various concentrations of L-NAME for 24 h. Cell lysates were subjected to immunoblotting for the detection of expression of several proteins. All experiments were repeated three times and the same results were obtained. C, Panc-1 cells were incubated with 1400W (100 μmol/L) and GSNO (500 μmol/L) for 24 h. Cell lysates were subjected to immunoblotting for the detection of expression of several proteins. All experiments were repeated three times and the same results were obtained.

Tris-HCl (pH 7.6), 150 mmol/L NaCl, 10 mmol/L sodium fluoride, 2 mmol/L sodium vanadate, 1 mmol/L phenyl-methylsulfonyl fluoride, 10 μg/mL aprotinin, 10 μg/mL leupeptin, 1 mmol/L DTT, and 1% NP40]. Following incubation on ice for 30 minutes, lysate samples were centrifuged at 13,000 × g for 30 minutes. Aliquots of the supernatant containing equal amounts of protein, determined using the Lowry assay, were subjected to immunoprecipitation followed by SDS-PAGE.

Immunoprecipitation and immunoblotting

Immunoprecipitation was done by incubating the lysates with antibody at 4°C for 18 hours. The immune complexes were collected by incubation with protein A/G-agarose beads for 1.5 hours at 4°C, washed three times with wash buffer [50 mmol/L Tris-HCl (pH 7.6), 150 mmol/L NaCl, 10 mmol/L sodium fluoride, 2 mmol/L sodium vanadate, 1 mmol/L phenylmethylsulfonyl fluoride, 10 μg/mL aprotinin, 10 μg/mL leupeptin, 1 mmol/L DTT, and 0.1% NP40], and boiled in Laemmli sample buffer.

Cell lysates containing equal amounts of either protein or immunoprecipitates were subjected to 7.5% or 10% SDS-PAGE after the addition of Laemmli sample buffer and boiling for 5 minutes. After transferring electrophoretically onto nitrocellulose membrane (Bio-Rad), the membranes were blocked in 5% nonfat dried milk for 2 hours at room temperature and incubated with primary

antibody for 2 hours at room temperature or overnight at 4°C. This was followed by incubation with secondary antibody conjugated with horseradish peroxidase for 1 hour at 4°C. Western blotting chemiluminescence luminol reagent (Perkin-Elmer) was used to visualize the blots. Bands of interest were scanned by using Power Look (UMAX Technologies) and were quantified by using NIH Image 1.62 software (NTIS).

Cell proliferation assay

To assess cell growth, MIAPaCa-2 and Panc-1 cells were seeded in 24-well plates (2 × 10^4 per well) in triplicates. The cells were preincubated for 24 hours in DMEM in the presence of 1% glutamine, 10% FBS, and antibiotics (1% penicillin and streptomycin sulfate) at 37°C under a humidified atmosphere of 5% CO_2 and were then exposed to various reagents for 24, 48, and 72 hours. The cells were collected and counted after being stained with 0.4% trypan blue (Sigma-Aldrich).

Cell invasion assay

The *in vitro* invasive potential of MIAPaCa-2 cells and Panc-1 cells was determined using BioCoat Matrigel Invasion Chambers (Becton Dickinson). According to the manufacturer's instructions, the Matrigel was hydrated with 0.5 mL of DMEM (serum-free) and incubated for 2 hours in humidified tissue culture incubator at 37°C under a humidified atmosphere of 5% CO_2. Evaluation

FIGURE 3 *Continued.* D, Panc-1 cells were incubated in DMEM with 10% FBS overnight and grown to 80% confluence. After incubation with 1400W (100 µmol/L) under serum starvation for 6 h, Panc-1 cells were incubated with IGF-I (25 nmol/L) for 5 min and then harvested. For the detection of IRS-1 phosphorylation, cell lysates were subjected to immunoprecipitation with anti–IRS-1 antibody followed by immunoblotting with anti-phosphotyrosine (PY) antibody. Then, cell lysates were directly subjected to immunoblotting. Data shown are the results of triplicate experiments. Bars, SEM. *, $P < 0.05$, compared with IGF-I only.
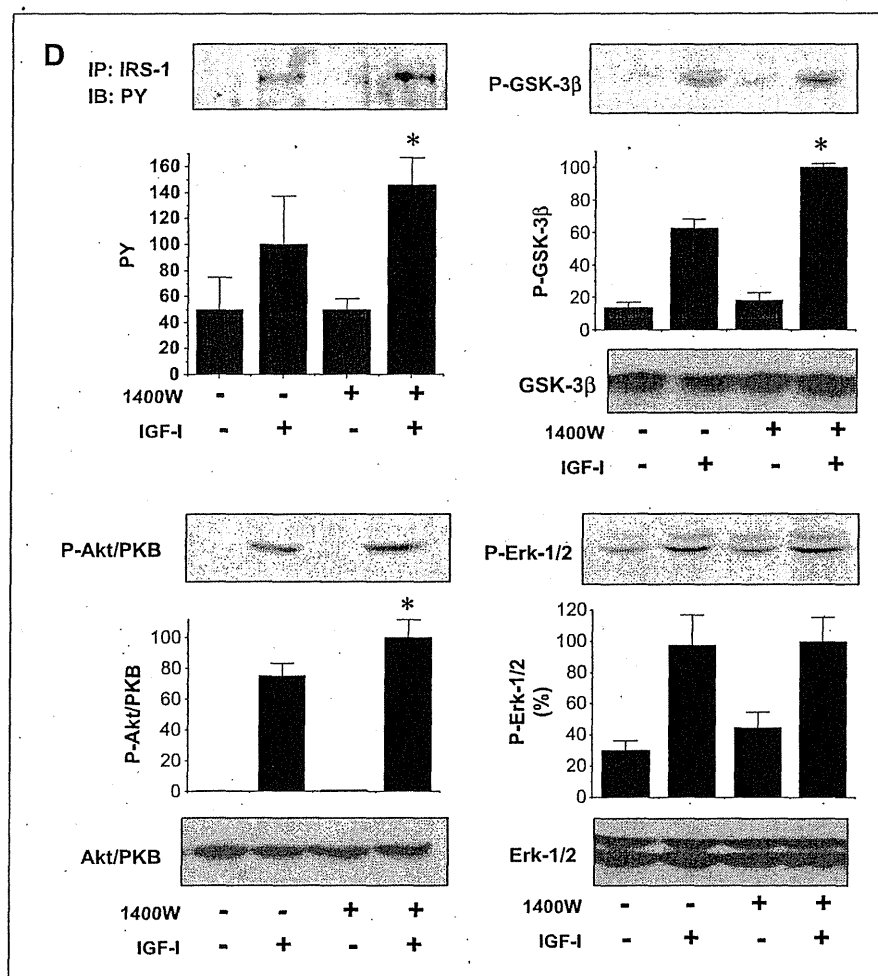
of cell migration used control inserts with 8.0-µm pores in 24-well plates. After detaching the cells with 0.25% trypsin and counting, they were diluted to 1.0×10^5 cells/mL in medium containing 1% FBS. A total of 0.5 $\times 10^5$ cells per well were placed on the top chamber of the insert above the medium containing chemoattractants, which was placed in the lower chamber. After incubation for 22 hours under a humidified atmosphere of 5% CO_2, the cells on the upper surface of the membrane were removed with a cotton swab and the migrated cells on the lower side of the membrane were fixed and stained using Diff-Quick (American Scientific Products) and counted in 10 random fields at ×100 magnification (30).

Statistical analysis

Data were compared using one-way ANOVA followed by Fisher's protected least significant difference test. $P < 0.05$ was considered statistically significant. All values were expressed as mean ± SEM.

Results

NO donors increase the concentration of nitrite (NO_2-) and 1400W inhibits nitrite production in the medium in which cancer cells are cultured

NO donors added to the culture medium provided NO to cancer cells. Cancer cells expressing iNOS protein can produce NO in normal conditions. We determined the concentration of nitrite, a metabolite of NO, in the culture medium. Both GSNO and SNAP, NO donors, augmented the concentration of nitrite in the culture medium in which MIAPaCa-2 cells were cultured for 6 and 24 hours (Fig. 1A). The concentration of nitrite was elevated with time in the medium in which Panc-1 cells were cultured. 1400W, a highly selective iNOS inhibitor, inhibited nitrite production in the culture medium at 3 and 6 hours (Fig. 1B).

NO influences insulin/IGF signals in MIAPaCa-2 cells

The stimulation of insulin or IGF-I resulted in remarkable tyrosine phosphorylation of insulin receptor, IGF-IR,

and IRS-1; phosphorylation of Akt/PKB at Ser[473] and GSK-3β at Ser[9]; and phosphorylation of Erk-1/2 in MIAPaCa-2 cells. SNAP, a NO donor, inhibited insulin-stimulated tyrosine phosphorylation of insulin receptor and IRS-1, phosphorylation of Akt/PKB at Ser[473], and phosphorylation of GSK-3β at Ser[9]. In addition, SNAP inhibited IGF-I–stimulated tyrosine phosphorylation of IGF-IR and IRS-1, phosphorylation of Akt/PKB at Ser[473], and phosphorylation of GSK-3β at Ser[9]. Furthermore, SNAP reduced IRS-1 protein expression, although this did not alter the expression of other proteins, including IGF-IR, Akt/PKB, GSK-3β, and Erk-1/2, in downstream of IGF signaling, as well as β-actin expression. On the other hand, SNAP induced the phosphorylation of Erk-1/2 without stimulation of insulin/IGF-I and enhanced insulin/IGF-I–stimulated phosphorylation of Erk-1/2; however, SNAP did not influence Erk-1/2 protein expression in MIAPaCa-2 cells (Fig. 1C and D). GSNO, a NO donor, inhibited IGF-I–induced phosphorylation of IGF-IR, IRS-1, and Akt/PKB, but enhanced the phosphorylation of Erk-1/2 as well as SNAP (Fig. 1E).

NO downregulates IRS-1 protein expression through proteasome-mediated degradation in MIAPaCa-2 cells

GSNO inhibited IRS-1 protein expression in MCF-7 as well as MIAPaCa-2 cells in a dose-dependent manner, but did not influence IRS-1 protein expression in MB 468 and Panc-1 cells, which exhibited less IRS-1 protein expression (Fig. 2A). The proteasome inhibitor MG132 completely reversed the reduction of IRS-1 protein expression by NO donors (GSNO and SNAP) in MIAPaCa-2 cells. Neither GSNO nor MG132 influenced GSK-3β and β-actin protein expression (Fig. 2B).

To further investigate IRS-1 protein degradation induced by NO donor, cDNA constructs of full-length IRS-1, IRS-1 DM1, IRS-1 DM2, and IRS-1 DM3 were produced and subcloned in mammalian expression vectors (Fig. 2C). MIAPaCa-2 cells were transfected with these expression vectors. GSNO reduced full-length IRS-1, IRS-1 DM1, and IRS-1 DM3 protein expression, although GSNO did not alter IRS-1 DM2 and β-actin protein expression (Fig. 2D). Ubiquitination of WT and mutated IRS-1 was detected by immunoprecipitation using anti-Flag antibody followed by immunoblotting with anti-ubiquitin. SNAP induced the ubiquitination of full-length IRS-1, IRS-1 DM1, and IRS-1 DM3, but did not induce the ubiquitination of IRS-1 DM2 (Fig. 2E). These results indicate that NO donor is capable of inducing ubiquitination at multiple sites in the COOH terminus of the IRS-1 protein.

iNOS protein is expressed in Panc-1 cells and 1400W upregulates IRS-1 protein expression and the IRS-1-Akt pathway in Panc-1 cells

iNOS protein was detected by immunoblotting in Panc-1 cells. IRS-1 protein expression was significantly increased by 1400W in a dose-dependent manner. However, Akt/PKB, β-actin, and Erk-1/2 protein expression was not al-

tered in Panc-1 cells (Fig. 3A). L-NAME, a nonselective NOS inhibitor, increased IRS-1 expression in Panc-1 cells, but it was not remarkable compared with the increase by 1400W (Fig. 3B). GSNO inhibited IRS-1 protein expression, upregulated by 1400W in Panc-1 cells (Fig. 3C). On the other hand, 1400W did not alter IRS-1 protein expression in MCF-7, which expresses high level of the protein (Supplementary Figure). 1400W enhanced IGF-I–stimulated tyrosine phosphorylation of IRS-1, phosphorylation of Akt/PKB at Ser[473], and phosphorylation of GSK-3β at Ser[9] in Panc-1 cells. In contrast, 1400W did not alter IGF-I–stimulated phosphorylation of Erk-1/2 (Fig. 3D). These results indicate that endogenous NO produced by iNOS plays a role in insulin/IGF-I signaling.

NO inhibits the proliferation of cancer cell lines and IRS-1 protein expression is associated with cancer cell proliferation

Cell proliferation assay revealed that 100 and 500 μmol/L GSNO inhibited the proliferation of MIAPaCa-2 and MCF-7 cells in culture medium containing 10% FBS (Fig. 4A). Mammalian cell expression vectors, pCMV Tag 4/IRS-1 (full-length), pCMV Tag 4/IRS-1 DM2, and pCMV Tag 4A vector alone, were transfected into MIAPaCa-2 and incubated with G418 for the selection of protein-expressing cells for more than 14 days. Subsequently, the cells expressing high levels of full-length IRS-1 protein or IRS-1 DM2 protein were cloned. Phosphorylation of Akt/PKB at Ser[473] and of GSK-3β at Ser[9] by stimulation of IGF-I were reduced in IRS-1 DM2–transfected cells in comparison with vector alone– or full-length IRS-1–transfected cells. SNAP failed to reduce the phosphorylation of Akt/PKB at Ser[473] and GSK-3β at Ser[9] by stimulation of IGF-I in IRS-1 DM2–transfected cells, but reduced their phosphorylation in vector alone– or full-length IRS-1–transfected cells. No difference was observed between these cell lines in terms of Akt/PKB and GSK-3β protein expression (Fig. 4B).

Proliferation of MIAPaCa-2 cells was elevated in culture medium containing serum or IGF-I, whereas no proliferation was observed in culture medium without serum or IGF-I. Proliferation of full-length IRS-1–transfected cells was greater than that of the vector alone–transfected cells in the culture medium containing 10% FBS. On the other hand, the proliferation of IRS-1 DM2–transfected cells was attenuated compared with full-length IRS-1 and vector alone (Fig. 4C). The proliferation of full-length IRS-1–transfected cells was greater than that of vector alone–transfected cells in the culture medium containing 100 nmol/L IGF-I without 10% FBS, whereas IGF-I–stimulated proliferation of IRS-1 DM2–transfected cells was not observed (Fig. 4D). GSNO (200 μmol/L) significantly reduced the proliferation of vector alone–, full-length IRS-1–, and IRS-1 DM2–transfected cells in culture medium containing 10% FBS or IGF-I. In the culture medium containing serum or IGF-I, the reduction rate of proliferation of full-length IRS-1–transfected cells was the greatest, whereas it was the least in IRS-1 DM2–transfected cells

(Fig. 4C and D). Proliferation of Panc-1 cells was not observed in the presence or absence of 1400W (100 μmol/L) when cultured without serum or IGF-I (Fig. 5A). 1400W significantly enhanced the proliferation of Panc-1 cells when cultured with 10% FBS (Fig. 5B). To further investigate the role of iNOS in IGF-I–stimulated proliferation, we evaluated the effects of the selective iNOS inhibitor 1400W in Panc-1 cells cultured with IGF-I in the absence of FBS. In the absence of 1400W, IGF-I failed to increase the cell numbers of Panc-1. The combination of IGF-I and 1400W, however, increased the number of Panc-1 cells (Fig. 5C). These results provide further evidence for the involvement of the downregulation of IGF-I signaling in NO-induced inhibition of cancer cell proliferation.

Sensitivity of invasion to NO is dependent on IGF signaling

In the invasion assay, there was no difference in invasion among vector alone–, full-length IRS-1–, and IRS-1 DM2–

transfected MIAPaCa-2 cells in the absence of the NO donor. The addition of 200 μmol/L GSNO remarkably reduced the invasion of vector alone– and full-length IRS-1–transfected MIAPaCa-2 cells, but did not alter the invasion of IRS-1 DM2–transfected MIAPaCa-2 cells (Fig. 6A and C). The invasion of Panc-1 cells incubated with 1400W (5 and 100 μmol/L) was significantly greater than that of Panc-1 cells incubated without 1400W (Fig. 6B and D).

Discussion

Here, we showed that NO donor reduced IRS-1 protein expression via proteasome-dependent degradation and inhibited insulin/IGF-I–stimulated phosphorylation of Akt/PKB and GSK-3β, but enhanced the phosphorylation of Erk-1/2 in pancreatic cancer cells. In this study, the COOH-terminal deletion mutants of IRS-1 (DM2) worked as a dominant negative, as previously reported (4). NO donor inhibited IGF-I–induced phosphorylation
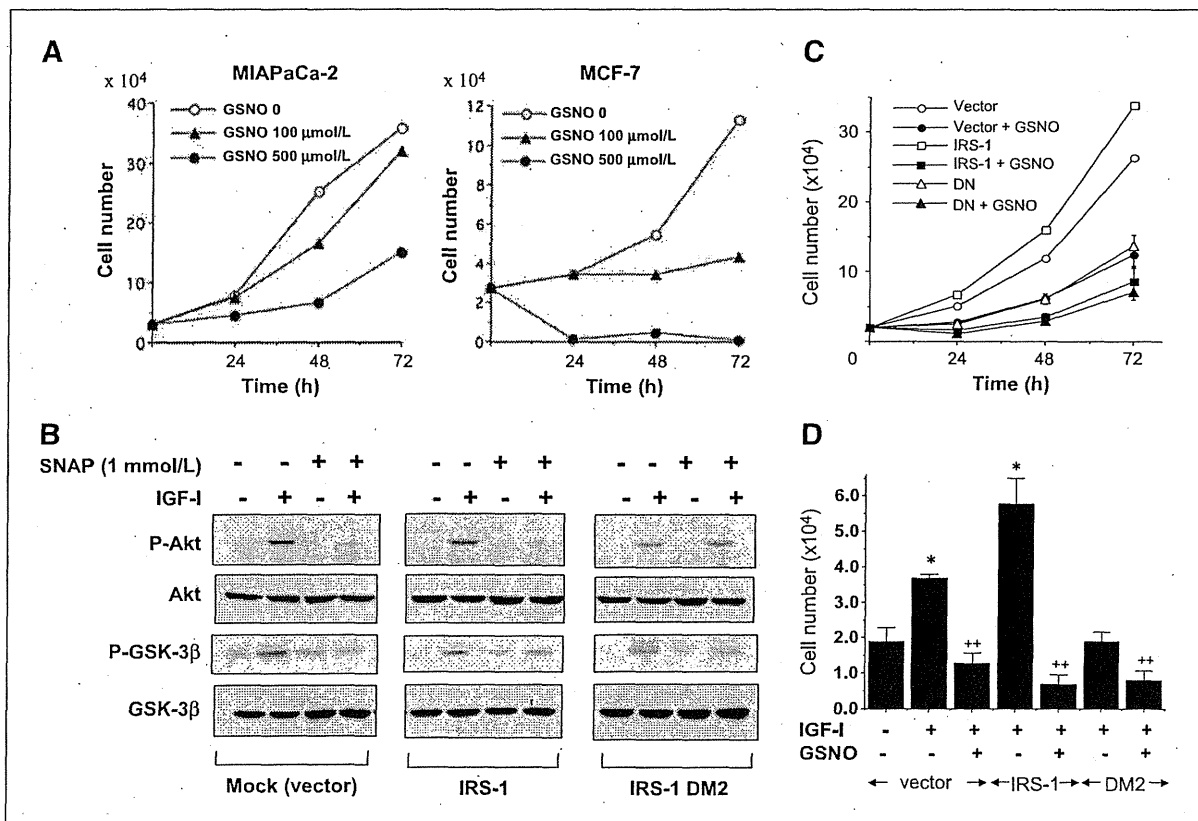
FIGURE 4. NO donor inhibits proliferation through downregulation of the IGF-Akt pathway in MIAPaCa-2 cells. A, MIAPaCa-2 and MCF-7 cells were incubated with GSNO (100 and 500 μmol/L) in medium containing 10% FBS for 24, 48, and 72 h. B, MIAPaCa-2 cells were transfected with vector only (as a mock), full-length IRS-1, and IRS-1 DM2 (as a dominant negative), followed by incubation with G418. Stable transfected cells were incubated in DMEM with 10% FBS overnight and grown to 80% confluence. After incubation with SNAP (1 mmol/L) under serum starvation for 6 h, the cells were incubated with IGF-I (25 nmol/L) for 5 min and then harvested. The cell lysates were subjected to immunoblotting. All experiments were repeated three times and the same results were obtained. C, stable transfected MIAPaCa-2 cells were incubated with GSNO (200 μmol/L) in medium containing 10% FBS for 24, 48, and 72 h. D, stable transfected cells (2 × 10⁴ per well) were incubated with GSNO (200 μmol/L) in medium with or without IGF-I (100 nmol/L; serum-free) for 48 h. *, P < 0.01, compared with control; ⁺⁺, P < 0.05, compared with IGF-I only.
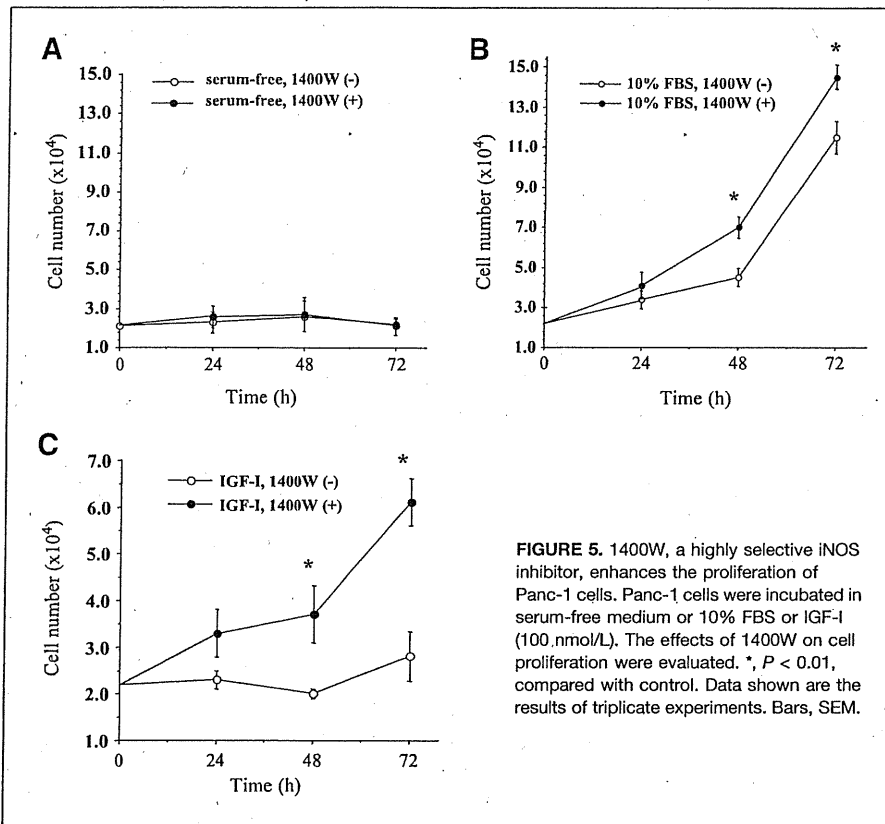
FIGURE 5. 1400W, a highly selective iNOS inhibitor, enhances the proliferation of Panc-1 cells. Panc-1 cells were incubated in serum-free medium or 10% FBS or IGF-I (100 nmol/L). The effects of 1400W on cell proliferation were evaluated. *, $P < 0.01$, compared with control. Data shown are the results of triplicate experiments. Bars, SEM.

of Akt/PKB and GSK-3β in MIAPaCa-2 cells transfected with IRS-1 WT or vector, but not in cells transfected with IRS-1 DM2, thus revealing the importance of IRS-1 in the inhibition of insulin/IGF signal by NO. IRS-1 expression and IGF-I signaling have important roles in the proliferation and invasion of MIAPaCa-2 cells and Panc-1 cells, consistent with previous reports on other cancer cells (3, 31-33). NO donor inhibited the IGF-I signaling, proliferation, and invasion of MIAPaCa-2 cells transfected with full-length IRS-1 or vector. In contrast, the selective iNOS inhibitor upregulated IRS-1 protein expression and insulin/IGF signal, resulting in enhanced proliferation and invasion activity in Panc-1 cells. These results indicate that the expression of IRS-1 protein is regulated by endogenous NO production by iNOS as well as exogenous NO, resulting in downregulation of IGF-I signaling and inhibition of the proliferation and invasion of MIAPaCa-2 and Panc-1 cancer cells.

Furthermore, we identified the COOH terminus as the site responsible for IRS-1 protein degradation by NO, which is located in the SH2-containing molecule binding site next to the phosphotyrosine binding (PTB) domain (Fig. 2C). The observation of the ubiquitination and degradation of both IRS-1 DM1 and IRS-1 DM3 indicates the possibility that there may be at least two sites responsible for NO donor–induced ubiquitination in the IRS-1 protein.

The mechanism explaining the degradation of the IRS-1 protein was previously reported (19, 34). Yu et al. showed that activated R-Ras induces degradation of IRS-1 protein associated with suppression of estrogen action in MCF-7 cells (34). However, in contrast to H-Ras and N-Ras, both of which contain Cys[118] residue in the conserved region, R-Ras not containing a Cys residue in the region is not modified by NO (35, 36). In addition, they described that R-Ras–dependent IRS-1 protein degradation was ubiquitin independent. Thus, R-Ras does not seem to contribute to NO-mediated IRS-1 degradation. We previously reported that PI3K, mammalian target of rapamycin, and c-jun NH_2-terminal kinase/stress-activated protein kinase inhibitors failed to block NO-induced IRS-1 protein reduction, despite having these inhibitors attenuated insulin-induced IRS-1 protein reduction in mouse C2C12 cells (19). Therefore, further investigation will be necessary to clarify the mechanism of NO-mediated ubiquitination and degradation of IRS-1.

In contrast to NO-induced downregulation of the IRS-1-PI3K-Akt pathway, NO donor upregulates the phosphorylation of Erk-1/2 in MIAPaCa-2 cells. These results are in accordance with previous studies reporting that NO modifies H-Ras and N-Ras directly by S-nitrosylation, resulting in the activation of the signaling (35, 37). Lim et al. showed that the PI3K-Akt pathway phosphorylates and

activates eNOS, resulting in the activity of H-Ras and N-Ras and tumor growth (36). In addition, other previous studies reported NO-induced cell proliferation and cell invasion (38, 39). The authors of these reports argue that NO-induced activation of Erk-1/2 leads to cell survival, in opposition to our data indicating the tumoricidal effects

of NO. However, in light of this discrepancy, we hypothesize that the outcome of cancer cells treated with NO may depend on the balance of the PI3K-Akt and Ras-Erk pathways. For instance, the rate of NO-induced inhibition of proliferation was highest in MIAPaCa-2 cells overexpressing full-length IRS-1, but minimal in cells expressing
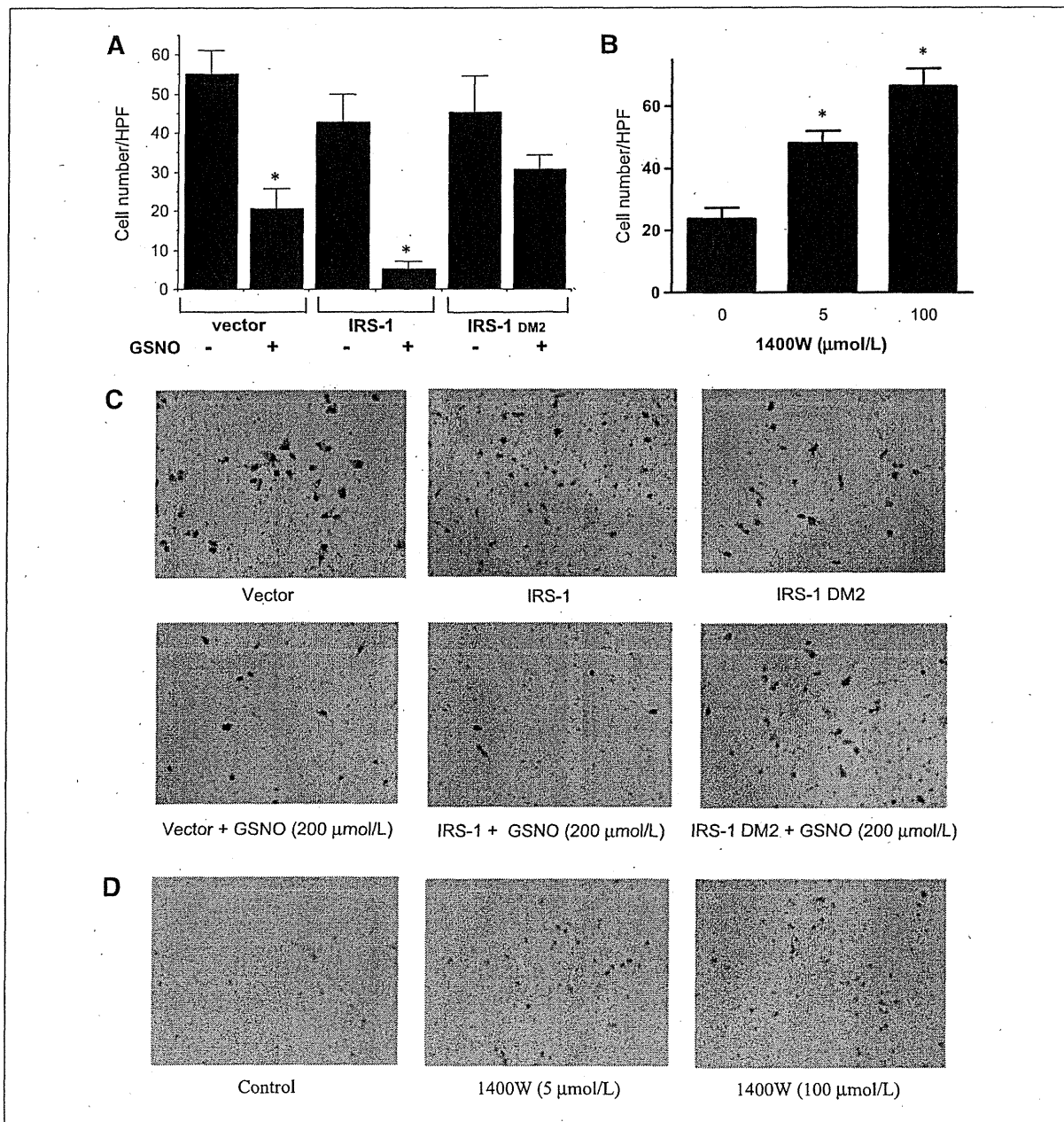
FIGURE 6. NO donor inhibits the invasion of MIAPaCa-2 cells and 1400W enhances the invasion of Panc-1 cells. Cell invasion was determined using BioCoat Matrigel Invasion Chambers. Stable transfected MIAPaCa-2 cells (A and C) or Panc-1 cells (B and D) were placed in the upper chambers. Conditioned medium of NIH 3T3 cells was used as a chemoattractant. Data shown are the results of triplicate experiments (A and B). Bars, SEM. C and D, representative staining of migrated cancer cells. *, $P < 0.01$, compared with control.

IRS-1 DM2. This means that MIAPaCa-2 cells overexpressing IRS-1 may be dependent on the IRS-1-Akt pathway, whereas MIAPaCa-2 cells overexpressing IRS-1 DM2 may be independent of the pathway.

NO donor exhibited minimal inhibition in the proliferation of stable IRS-1 DM2–transfected MIAPaCa-2 cells, although NO donor failed to reduce the invasion of the cells. These results indicate that NO may downregulate the proliferation of MIAPaCa-2 cells partially through mechanisms other than the reduction of IRS-1 protein expression and phosphorylation. Namely, as previously reported, NO donor inhibits the activity of Akt/PKB through S-nitrosylation (12), indicating the possibility that it may be one of several mechanisms. Furthermore, NO induced DNA damage, and the activation of p53 and mitogen-activated protein kinase may be related to the phenomenon, as reported previously by Hofseth et al. (40).

This study shows that GSNO and SNAP provide high concentration of nitrite in the culture medium at 6 hours after administration. Furthermore, Panc-1 cells produced nitrite, a metabolite of NO, in culture medium. The level of NO in the cells is an important factor that influences the pathophysiologic activity of NO. iNOS can provide high concentrations of NO in Panc-1 cells, and NO derived from 100 to 500 μmol/L GSNO and 1 mmol/L SNAP may result in a high NO concentration in the cytosol of cancer cells. High levels of NO have been shown to exhibit cytotoxicity in various cells (41). Because the half time in which GSNO provides NO is longer than that of SNAP, we intentionally used SNAP for short-term experiments and GSNO for long-term experiments (42, 43). GSNO inhibited IRS-1 protein expression at dosages of

100 to 200 μmol/L. These dosages of GSNO also inhibited cell proliferation and invasion. These findings suggest that NO-mediated IRS-1 degradation contributes to the inhibition of cell proliferation and invasion by NO donor. GSNO reduces IRS-1 protein expression, which is upregulated by 1400W in Panc-1 cells (Fig. 3C). These results suggest that endogenous NO is sufficient to reduce IRS-1 expression; therefore, GSNO does not reduce IRS-1 expression in Panc-1 cells without 1400W.

The usefulness of cancer therapy using NO, including iNOS gene therapy and administration of NO donor, was recently confirmed in animal models (44-46). Consequently, NO therapy has been focused on and is currently undergoing clinical evaluation for cancer prevention (47). However, the molecular mechanism still remains unclear. Our data suggest that NO-induced downregulation of the insulin/IGF-IRS-1-Akt pathway may play an important role in the proliferation and invasion of pancreatic cancer cells.

Disclosure of Potential Conflicts of Interest

No potential conflicts of interest were disclosed.

Grant Support

References

1. Bergmann U, Funatomi H, Yokoyama M, Beger HG, Korc M. Insulin-like growth factor I overexpression in human pancreatic cancer: evidence for autocrine and paracrine roles. Cancer Res 1995;55: 2007–11.

2. Furukawa M, Raffeld M, Mateo C, et al. Increased expression of insulin-like growth factor I and/or its receptor in gastrinomas is associated with low curability, increased growth, and development of metastases. Clin Cancer Res 2005;11:3233–42.

3. Kim HJ, Litzenburger BC, Cui X, et al. Constitutively active type I insulin-like growth factor receptor causes transformation and xenograft growth of immortalized mammary epithelial cells and is accompanied by an epithelial-to-mesenchymal transition mediated by NF-κB and snail. Mol Cell Biol 2007;27:3165–75.

4. Tanaka S, Wands JR. A carboxy-terminal truncated insulin receptor substrate-1 dominant negative protein reverses the human hepatocellular carcinoma malignant phenotype. J Clin Invest 1996;98: 2100–8.

5. Ito T, Sasaki Y, Wands JR. Overexpression of human insulin receptor substrate 1 induces cellular transformation with activation of mitogen-activated protein kinases. Mol Cell Biol 1996;16:943–51.

6. Chang Q, Li Y, White MF, Fletcher JA, Xiao S. Constitutive activation of insulin receptor substrate 1 is a frequent event in human tumors: therapeutic implications. Cancer Res 2002;62:6035–8.

7. Asano T, Yao Y, Shin S, McCubrey J, Abbruzzese JL, Reddy SA. Insulin receptor substrate is a mediator of phosphoinositide 3-kinase activation in quiescent pancreatic cancer cells. Cancer Res 2005;65: 9164–8.

8. Dearth RK, Cui X, Kim HJ, et al. Mammary tumorigenesis and

metastasis caused by overexpression of insulin receptor substrate 1 (IRS-1) or IRS-2. Mol Cell Biol 2006;26:9302–14.

9. Park HS, Huh SH, Kim MS, Lee SH, Choi EJ. Nitric oxide negatively regulates c-Jun N-terminal kinase/stress-activated protein kinase by means of S-nitrosylation. Proc Natl Acad Sci U S A 2000;97: 14382–7.

10. Reynaert NL, Ckless K, Korn SH, et al. Nitric oxide represses inhibitory κB kinase through S-nitrosylation. Proc Natl Acad Sci U S A 2004;101:8945–50.

11. Mannick JB, Hausladen A, Liu L, et al. Fas-induced caspase denitrosylation. Science 1999;284:651–4.

12. Yasukawa T, Tokunaga E, Ota H, Sugita H, Martyn JA, Kaneki M. S-nitrosylation-dependent inactivation of Akt/protein kinase B in insulin resistance. J Biol Chem 2005;280:7511–8.

13. Ignarro LJ, Buga GM, Wood KS, Byrns RE, Chaudhuri G. Endothelium-derived relaxing factor produced and released from artery and vein is nitric oxide. Proc Natl Acad Sci U S A 1987;84:9265–9.

14. Palmer RM, Ferrige AG, Moncada S. Nitric oxide release accounts for the biological activity of endothelium-derived relaxing factor. Nature 1987;327:524–6.

15. Kuo PC, Schroeder RA. The emerging multifaceted roles of nitric oxide. Ann Surg 1995;221:220–35.

16. Wink DA, Miranda KM, Espey MG. Effects of oxidative and nitrosative stress in cytotoxicity. Semin Perinatol 2000;24:20–3.

17. Perreault M, Marette A. Targeted disruption of inducible nitric oxide synthase protects against obesity-linked insulin resistance in muscle. Nat Med 2001;7:1138–43.

18. Xie K, Fidler IJ. Therapy of cancer metastasis by activation of

the inducible nitric oxide synthase. Cancer Metastasis Rev 1998;17:
55–75.

19. Sugita H, Fujimoto M, Yasukawa T, et al. Inducible nitric-oxide synthase and NO donor induce insulin receptor substrate-1 degradation in skeletal muscle cells. J Biol Chem 2005;280:14203–11.

20. Ambs S, Merriam WG, Ogunfusika MO, et al. p53 and vascular endothelial growth factor regulate tumor growth of NOS2-expressing human carcinoma cells. Nat Med 1998;4:1371–6.

21. Camp ER, Yang A, Liu W, et al. Roles of nitric oxide synthase inhibition and vascular endothelial growth factor receptor-2 inhibition on vascular morphology and function in an in vivo model of pancreatic cancer. Clin Cancer Res 2006;12:2628–33.

22. Kalivendi SV, Kotamraju S, Zhao H, Joseph J, Kalyanaraman B. Doxorubicin-induced apoptosis is associated with increased transcription of endothelial nitric-oxide synthase. Effect of antiapoptotic antioxidants and calcium. J Biol Chem 2001;276:47266–76.

23. Wang B, Wei D, Crum VE, et al. A novel model system for studying the double-edged roles of nitric oxide production in pancreatic cancer growth and metastasis. Oncogene 2003;22:1771–82.

24. Peshes-Yaloz N, Rosen D, Sondel PM, Krammer PH, Berke G. Up-regulation of Fas (CD95) expression in tumour cells in vivo. Immunology 2007;120:502–11.

25. Kotamraju S, Williams CL, Kalyanaraman B. Statin-induced breast cancer cell death: role of inducible nitric oxide and arginase-dependent pathways. Cancer Res 2007;67:7386–94.

26. Notas G, Nifli AP, Kampa M, Vercauteren J, Kouroumalis E, Castanas E. Resveratrol exerts its antiproliferative effect on HepG2 hepatocellular carcinoma cells, by inducing cell cycle arrest, and NOS activation. Biochim Biophys Acta 2006;1760:1657–66.

27. Jarry A, Charrier L, Bou-Hanna C, et al. Position in cell cycle controls the sensitivity of colon cancer cells to nitric oxide-dependent programmed cell death. Cancer Res 2004;64:4227–34.

28. Chawla-Sarkar M, Bauer JA, Lupica JA, et al. Suppression of NF-κB survival signaling by nitrosylcobalamin sensitizes neoplasms to the anti-tumor effects of Apo2L/TRAIL. J Biol Chem 2003;278:39461–9.

29. Misko TP, Schilling RJ, Salvemini D, Moore WM, Currie MG. A fluorometric assay for the measurement of nitrite in biological samples. Anal Biochem 1993;214:11–6.

30. Ceyhan GO, Giese NA, Erkan M, et al. The neurotrophic factor artemin promotes pancreatic cancer invasion. Ann Surg 2006;244:274–81.

31. Shi B, Sepp-Lorenzino L, Prisco M, Linsley P, deAngelis T, Baserga R. Micro RNA 145 targets the insulin receptor substrate-1 and inhibits the growth of colon cancer cells. J Biol Chem 2007;282:32582–90.

32. Scamuffa N, Siegfried G, Bontemps Y, et al. Selective inhibition of proprotein convertases represses the metastatic potential of human colorectal tumor cells. J Clin Invest 2008;118:352–63.

33. Jiang P, Enomoto A, Jijiwa M, et al. An actin-binding protein Girdin

regulates the motility of breast cancer cells. Cancer Res 2008;68:1310–8.

34. Yu Y, Hao Y, Feig LA. The R-Ras GTPase mediates cross talk between estrogen and insulin signaling in breast cancer cells. Mol Cell Biol 2006;26:6372–80.

35. Lander HM, Hajjar DP, Hempstead BL, et al. A molecular redox switch on p21(ras). Structural basis for the nitric oxide-p21(ras) interaction. J Biol Chem 1997;272:4323–6.

36. Lim KH, Ancrile BB, Kashatus DF, Counter CM. Tumour maintenance is mediated by eNOS. Nature 2008;452:646–9.

37. Ibiza S, Perez-Rodriguez A, Ortega A, et al. Endothelial nitric oxide synthase regulates N-Ras activation on the Golgi complex of antigen-stimulated T cells. Proc Natl Acad Sci U S A 2008;105:10507–12.

38. Ellerhorst JA, Ekmekcioglu S, Johnson MK, Cooke CP, Johnson MM, Grimm EA. Regulation of iNOS by the p44/42 mitogen-activated protein kinase pathway in human melanoma. Oncogene 2006;25:3956–62.

39. Donnini S, Finetti F, Solito R, et al. EP2 prostanoid receptor promotes squamous cell carcinoma growth through epidermal growth factor receptor transactivation and iNOS and ERK1/2 pathways. FASEB J 2007;21:2418–30.

40. Hofseth LJ, Saito S, Hussain SP, et al. Nitric oxide-induced cellular stress and p53 activation in chronic inflammation. Proc Natl Acad Sci U S A 2003;100:143–8.

41. Heller R, Polack T, Grabner R, Till U. Nitric oxide inhibits proliferation of human endothelial cells via a mechanism independent of cGMP. Atherosclerosis 1999;144:49–57.

42. Mancuso C, Bonsignore A, Di Stasio E, Mordente A, Motterlini R. Bilirubin and S-nitrosothiols interaction: evidence for a possible role of bilirubin as a scavenger of nitric oxide. Biochem Pharmacol 2003;66:2355–63.

43. Janssens MY, Verovski VN, Van den Berge DL, Monsaert C, Storme GA. Radiosensitization of hypoxic tumour cells by S-nitroso-N-acetylpenicillamine implicates a bioreductive mechanism of nitric oxide generation. Br J Cancer 1999;79:1085–9.

44. Adams C, McCarthy HO, Coulter JA, et al. Nitric oxide synthase gene therapy enhances the toxicity of cisplatin in cancer cells. J Gene Med 2009;11:160–8.

45. Kiziltepe T, Hideshima T, Ishitsuka K, et al. JS-K, a GST-activated nitric oxide generator, induces DNA double-strand breaks, activates DNA damage response pathways, and induces apoptosis in vitro and in vivo in human multiple myeloma cells. Blood 2007;110:709–18.

46. Wang Z, Cook T, Alber S, et al. Adenoviral gene transfer of the human inducible nitric oxide synthase gene enhances the radiation response of human colorectal cancer associated with alterations in tumor vascularity. Cancer Res 2004;64:1386–95.

47. Ma Q, Wang Y, Gao X, Ma Z, Song Z. L-Arginine reduces cell proliferation and ornithine decarboxylase activity in patients with colorectal adenoma and adenocarcinoma. Clin Cancer Res 2007;13:7407–12.

Relationship of strain-dependent susceptibility to experimentally induced acute pancreatitis with regulation of Prss1 and Spink3 expression

Jun Wang[1], Masaki Ohmuraya[1,2,3], Koichi Suyama[1,3], Masahiko Hirota[3], Nobuyuki Ozaki[1,3], Hideo Baba[3], Naomi Nakagata[4], Kimi Araki[1] and Ken-ichi Yamamura[1]

To analyze susceptibility to acute pancreatitis, five mouse strains including Japanese Fancy Mouse 1 (JF1), C57BL/6J, BALB/c, CBA/J, and C3H/HeJ were treated with either a cholecystokinin analog, cerulein, or a choline-deficient, ethionine-supplemented (CDE) diet. The severity of acute pancreatitis induced by cerulein was highest in C3H/HeJ and CBA/J, moderate in BALB/c, and mildest in C57BL/6J and JF1. Basal protein expression levels of the serine protease inhibitor, Kazal type 3 (Spink3) were higher in JF1 and C57BL/6J mice than those of the other three strains under normal feeding conditions. After treatment with cerulein, expression level of Spink3 increased remarkably in JF1 and mildly in C57BL/6J, BALB/c, CBA/J, and C3H/HeJ strains. Increased proteinase, serine, 1 (Prss1) protein expression accompanied by increased trypsin activity with cerulein treatment was observed in susceptible strains such as CBA/J and C3H/HeJ. Similar results were obtained with a CDE diet. In the 3 kb Spink3 promoter region, 92 or 8 nucleotide changes were found in JF1 or C3H vs C57BL/6J, respectively, whereas in the Prss1 promoter region 39 or 46 nucleotide changes were found in JF1 or C3H vs C57BL/6J, respectively. These results suggest that regulation of Prss1 and Spink3 expression is involved in the susceptibility to experimentally induced pancreatitis. The JF1 strain, which is derived from the Japanese wild mouse, will be useful to examine new mechanisms that may not be found in other laboratory mouse strains.

Laboratory Investigation (2010) 90, 654–664; doi:10.1038/labinvest.2010.44; published online 15 February 2010

Over 450 inbred strains of mice have been described,[1] providing a wealth of different genotypes and phenotypes for studying human diseases. Actually, the use of various breeding strategies in combination with positional cloning and positional candidate gene approach has led to the discovery of many genes that underlie human disease.[2] The Japanese wild mouse, belonging to *Mus musculus molossinus*, has several genetic characteristics clearly distinguishable from the European wild mouse, derived from *M.m. domesticus*. These subspecies were separated about one million years ago and about 1% of their genome sequences are different.[3–8] Therefore, strains MSM/Ms[9] and Japanese Fancy Mouse 1 (JF1),[10] which were established from *M.m. molossinus*, are powerful genetic resources to analyze disease processes.

Many inbred strains have been bred for specific phenotypes. C57BL/6J mice are susceptible to high-fat diet-induced

type II diabetes.[11] JF1 mice are especially sensitive to high-fat diet-induced diabetes and obesity, whereas MSM/Ms mice are resistant.[12] To date, however, there is little information about the difference in severity of pancreatitis among inbred strains of mice.

Acute pancreatitis is an important disease that can be triggered by a variety of factors, including excessive alcohol consumption,[13–16] obstruction of the ampulla of Vater by gall stones,[17,18] and genetic factors.[19,20] Hereditary chronic pancreatitis is a rare form of early onset chronic pancreatitis, characterized by the onset of recurrent attacks of acute pancreatitis in childhood, and frequently progresses to chronic pancreatitis. One type of the hereditary pancreatitis is caused by a mutation in the proteinase, serine, 1 (PRSS1) gene, encoding cationic trypsinogen. PRSS1 mutation results in an amino-acid substitution in the autolytic domain of

[1]Division of Developmental Genetics, Institute of Molecular Embryology and Genetics, Kumamoto University, Kumamoto, Japan; [2]Priority Organization for Innovation and Excellence, Kumamoto University, Kumamoto, Japan; [3]Department of Gastroenterological Surgery, Kumamoto University, Kumamoto, Japan and [4]Center for Animal Resources and Development, Institute of Resource Development and Analysis, Kumamoto University, Kumamoto, Japan
Correspondence: Dr K-i Yamamura, MD, PhD, Institute of Molecular Embryology and Genetics, Kumamoto University, 2-2-1 Honjo, Kumamoto 860-0811, Japan.
E-mail: yamamura@gpo.kumamoto-u.ac.jp

trypsin. Thus, the mutation blocks autolysis and results in continuous trypsin activity.[21,22] In addition, mutation of the trypsin-specific inhibitor, serine protease inhibitor, Kazal type 1 (SPINK1), has been found to be associated with chronic pancreatitis as well.[23] We earlier showed that Spink3 (mouse homolog of human SPINK1) has dual functions for trypsin inhibition: one as a trypsin inhibitor by direct binding to trypsin[24] and another as a suppressor of autophagy, which is involved in trypsinogen activation.[25,26] In summary, mutations in PRSS1[27] and SPINK1[19] genes are acknowledged as genetic risk factors for pancreatitis in human patients.

To address whether genetic background can affect the development of acute pancreatitis in relation to expression of Prss1 and Spink3, the susceptibility of acute pancreatitis was compared among five inbred mouse strains including JF1 in two models of experimental acute pancreatitis, cerulein-induced and choline-deficient ethionine-supplemented (CDE) diet-induced acute pancreatitis. We found that there were significant differences in susceptibility to acute pancreatitis among mouse strains, and that susceptibility to acute pancreatitis was negatively or positively related with expression levels of Spink3 or Prss1, respectively. In addition, sequence differences in Spink3 promoter regions between JF1 and other strains were considered to be involved in differences in expression levels.

MATERIALS AND METHODS
Mouse Strains
All procedures were approved by the Animal Care and Use Committee of Kumamoto University. The five mouse strains were used in the following experiments: JF1 (Riken BioResource Center, Tsukuba, Japan), C57BL/6J, CBA/J, and BALB/c (CLEA Japan, Inc. Tokyo, Japan), and C3H/HeJ (Charles River Laboratories Japan, Inc. Yokohama, Japan). For every experiment, five mice in each strain were assigned to either a control or experimental group.

Cerulein-Induced Pancreatitis
After an overnight fast, mice were given hourly intraperitoneal injections of either saline (control) or cerulein (50 µg/kg) (Sigma-Aldrich Corp, Tokyo, Japan) for 12 h. One hour after the last injection, serum and the pancreas were isolated for the following studies.

CDE Diet-Induced Pancreatitis
Composition of CDE chow was described earlier.[28] Mice were fasted for 24 h and then fed with either CDE or control (regular laboratory chow) diet for 72 h. Then, animals were fed with regular laboratory chow for 12 h before they were killed.

Histological Examination and Pathologic Scoring
For histological analysis, pancreatic tissue was fixed overnight in 10% formalin, embedded in paraffin, sectioned, and stained with hematoxylin and eosin. The extent of injury was estimated using a method described earlier with some minor modifications.[29] Briefly, 10 randomly chosen microscopic fields were examined for each pancreas specimen, and the total surface of the slide was scored for five different variables determining severity of inflammation: edema (E), hemorrhage (H), inflammatory cell infiltration (I), acinar cell vacuolization (V), and acinar cell necrosis (N). Total scores for these five parameters were obtained in each group after mapping the pancreas into 10 fields and evaluating each field independently.

Serum Amylase Activity
Mouse blood was used to measure pancreatic amylase activity using substrate, 2-chloro-4-nitrophenyl-4-galactopyranosylmaltoside (Gal-G2-CNP) (CicaLiquid-N p-AMY, Kanto Chemical Co., Inc. Tokyo, Japan).

Measurement of Trypsin Activity
Measurement of trypsin activity was performed as described earlier.[25]

Northern Blot Analysis
Total RNAs were extracted from the pancreas with Sepasol (Nacalai Tesque, Kyoto, Japan). For making digoxigenin-labeled RNA probes (Roche Molecular Biochemicals, Germany), mouse Spink3 and Prss1 probes were derived from mouse pancreas RNA by reverse transcriptase PCR using the following nucleotide sequences: mPsti1 (agttcttctggcttttgcaccc) and mPsti26 (cccacgttgcctttcattacgg); Prss1: mPrss1-s1 (taaaggcaggcttccatccagg) and mPrss1-a1 (tgacagtgactgcagagggatt). cDNA was subsequently subcloned into a pGEM-T easy vector (Promega, Madison, WI, USA).

Sequence Analysis
Both cDNAs and the promoter regions of Spink3 and Prss1 gene were amplified by PCR using TaKaRa LA Taq polymerase mix (Takara Bio Inc., Kyoto, Japan). Primers used in the RT–PCR included the following sequences: mPsti1 (agttcttctggcttttgcaccc) and mPsti26 (cccacgttgcctttcattacgg) for Spink3; mPrss1-s1 (taaaggcaggcttccatccagg) and mPrss1-a1 (tgacagtgactgcagagggatt) for Prss1. Three pairs of primers were applied to sequence the 3 kb promoter region of each gene. Sequencing was performed using the Big Dye Terminator Cycle Sequencing ready kit and an ABI 310 Genetic Analyzer (Applied Biosystems).

Western Blot Analysis
Western blot analysis was carried out according to the method described earlier.[25] Primary antibodies to the following antigens were used at the indicated dilutions: Spink3 (Transgenic Inc., Kumamoto, Japan), 1:1000; Prss1 (Nordic immunological laboratories, Tilburg, Netherlands), 1:1000; amylase (Santa Cruz Biotechnology, CA, USA), 1:1000; and light chain 3 (LC3) (MBL International, Woburn, MA, USA),

1:1000. An anti-rabbit secondary immunoglobulin G anti-body conjugated with horseradish peroxidase (Amersham Biosciences Corp, Piscataway, NJ, USA) was used to detect all proteins. Intensities of the bands were quantified by densitometry using ImageJ software (version 1.38, a program inspired by NIH image; http://rsb.info.nih.gov/ij/docs/index.html).

Statistical Analysis

All values are presented as mean ± s.d. (range, 95% CI), and statistical analysis was performed applying unpaired Student's t-tests. $P < 0.05$ was considered to be a statistically significant difference.

RESULTS
Cerulein-Induced Pancreatitis

The pancreas of all strains of mice injected with normal saline showed no histological changes, whereas cerulein treatment induced variable degrees of acute pancreatitis among these five strains (Figure 1). C57BL/6J mice showed the mildest pancreatitis (Figure 1g and h), whereas C3H/HeJ mice displayed the most severe pancreatitis (Figure 1s and t). BALB/c and CBA/J mice showed a moderate degree of pancreatitis (Figure 1k, l, o and p). Acute pancreatitis in JF1 mice was obviously milder than pancreatitis in BALB/c and CBA/J mice, yet more severe than C57BL/6J with evidence of acinar cell necrosis (Figure 1c). Further calculations of semi-quantitative pathologic scores and statistical analysis strongly supported this statistical difference in susceptibility (Figure 1u and v). Levels of amylase coincide with histological findings, highest in C3H/HeJ, followed by CBA/J and BALB/c, and lowest in C57BL/6J and JF1 with statistically significant differences ($P < 0.05$) (Figure 1w). Interestingly, serum levels of amylase in JF1 mice were lowest in spite of the presence of low grade of acinar cell necrosis when compared with C57BL/6J mice.

CDE Diet-Induced Pancreatitis

In CDE diet-induced pancreatitis, the general histological appearance of pancreatic tissues was much milder than those in cerulein-induced pancreatitis. Acinar cells presented almost no obvious histological changes in JF1, C57BL/6J or BALB/c mice (Figure 2c, d, g, h, k and l). C3H/HeJ mice, however, showed signs of obvious necrosis in acinar cells together with infiltration of inflammatory cells and slight vacuolization of acinar cells (Figure 2s and t). A mild degree of acinar cell necrosis was observed in CBA/J mice (Figure 2o and p). Peripancreatic hemorrhage was a frequent sign observed in this model as shown in Figure 2l, whereas fewer inflammatory cells were found within the pancreatic interstitium (Figure 2s). Pathologic scores were quite consistent to the microscopically gross observation (Figure 2u and w). Levels of serum amylase were proportional to these histological findings (Figure 2w).

Basal Expression Levels of Spink3 in Mice under Normal Feeding

Basal expression levels of Spink3 without induction were examined by western blot analysis in each strain of mice. Interestingly, results showed that expression of Spink3 was statistically higher in JF1 and C57BL/6J than the other three strains of mice that were susceptible to pancreatitis (Supplementary Figure 1).

Expression of Spink3 and Prss1 after Treatment with Cerulein

We examined the levels of mRNA and protein expressions of Spink3 and Prss1 without and with cerulein treatment. Without induction, CBA/J mice had lower Spink3 mRNA levels than those in other strains (Figure 3a and b). With cerulein treatment, Spink3 mRNA expression significantly increased in JF1, mildly in C57BL/6J, but decreased in BALB/c and C3H/HeJ strains (Figure 3a and c).
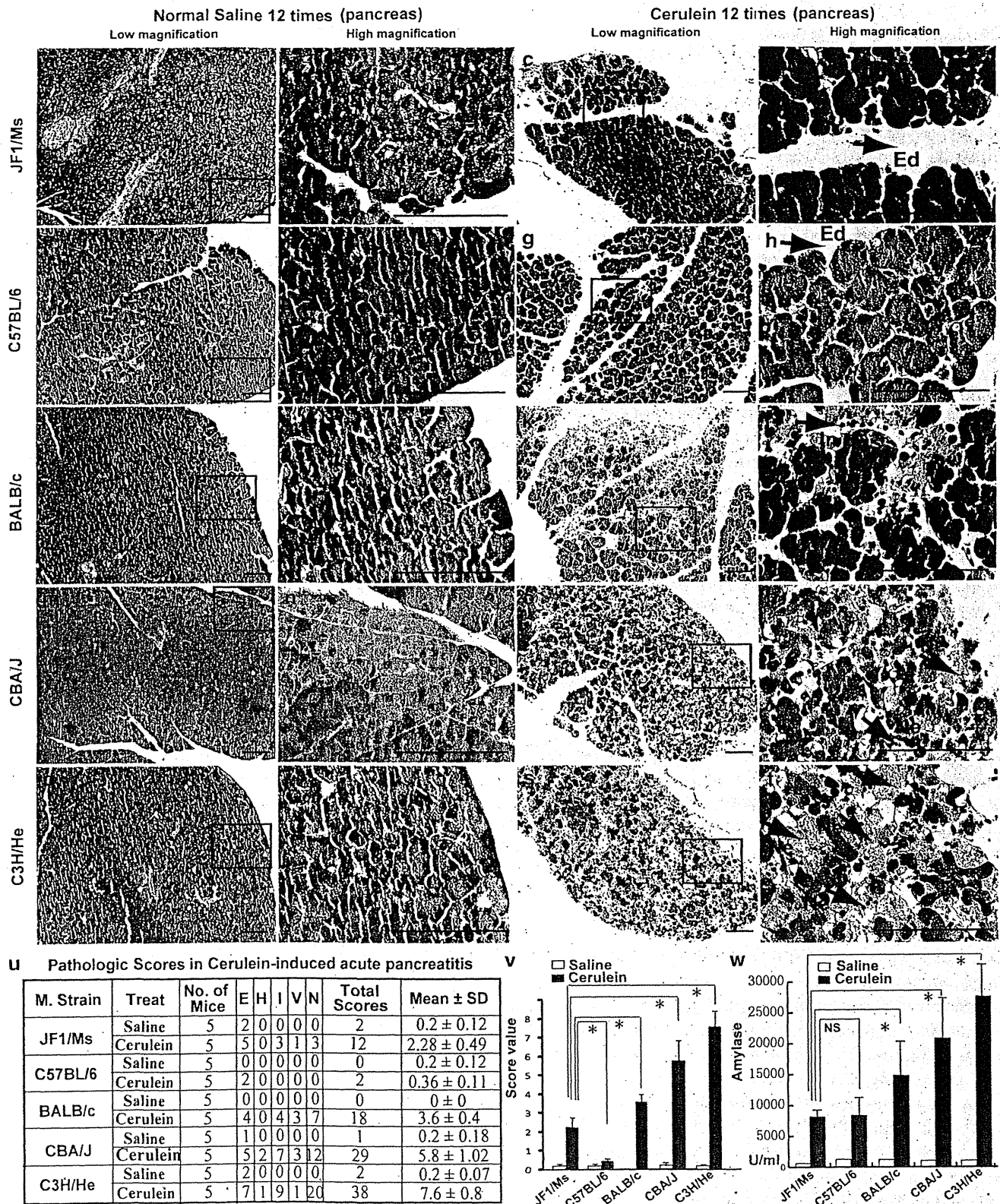
Without cerulein treatment, BALB/c mice had higher Prss1 mRNA levels than those in other strains (Figure 3a and b). After cerulein treatment, Prss1 mRNA levels in JF1, C57BL/6J, and BALB/c remained unchanged, but decreased in CBA/J and C3H/HeJ mice (Figure 3a and c). Expression G3PDH was notably augmented with cerulein treatment (Figure 3a), suggesting that this gene expression could not be used as reference loading control. Thus, we used 18S or 28S rRNA as reference RNAs.

Then, protein expression for Spink3 and Prss1 was examined by western blot analyses. Notably, Spink3 levels in JF1 mice decreased after overnight starvation (Figure 3e) when compared with normal feeding (see Supplementary Figure 1), although levels in other strains were unchanged after starvation. Without treatment, levels of Spink3 in C57BL/6J mice were higher than those in the other four strains (Figure 3d and e). With cerulein treatment, Spink3 expression was increased significantly in JF1, moderately in C57BL/6J and BALB/c, and slightly in CBA/J and C3H/HeJ (Figure 3d and f).

The level of Prss1 protein expression was lower in CBA/J and C3H/HeJ than those in the other three strains without induction (Figure 3d and e). However, levels of Prss1 increased significantly in BALB/c, CBA/J, and C3H/HeJ with cerulein treatment, whereas no notable changes were observed in JF1 and C57BL/6 strains (Figure 3d and f). Taken together, these results suggest that induction levels of Spink3 and Prss1 were negatively and positively related to susceptibility of cerulein-induced pancreatitis, respectively.

Expression of Spink3 and Prss1 with CDE Diet

When given a normal diet, levels of Spink3 mRNA in C57BL/6, CBA/J, and C3H/HeJ mice were higher than those in JF1 and BALB/c (Figure 4a and b). In the CDE diet model, Spink3 mRNA expression was significantly increased in JF1 mice, but mildly increased in C57BL/6J and CBA/J (Figure 4a and c).

Normal Saline 12 times (pancreas)

Low magnification High magnification

Cerulein 12 times (pancreas)

Low magnification High magnification

U **Pathologic Scores in Cerulein-induced acute pancreatitis**

M. Strain	Treat	No. of Mice	E	H	I	V	N	Total Scores	Mean ± SD
JF1/Ms	Saline	5	2	0	0	0	0	2	0.2 ± 0.12
	Cerulein	5	5	0	3	1	3	12	2.28 ± 0.49
C57BL/6	Saline	5	0	0	0	0	0	0	0.2 ± 0.12
	Cerulein	5	2	0	0	0	0	2	0.36 ± 0.11
BALB/c	Saline	5	0	0	0	0	0	0	0 ± 0
	Cerulein	5	4	0	4	3	7	18	3.6 ± 0.4
CBA/J	Saline	5	1	0	0	0	0	1	0.2 ± 0.18
	Cerulein	5	5	2	7	3	12	29	5.8 ± 1.02
C3H/He	Saline	5	2	0	0	0	0	2	0.2 ± 0.07
	Cerulein	5	7	1	9	1	20	38	7.6 ± 0.8

Figure 1 Histological changes, pathologic scores, and serum amylase levels in pancreas with and without cerulein treatment. (a, b, e, f, i, j, m, n, q, r) Saline-treated mice. (c, d, g, h, k, l, o, p, s, t) Cerulein-treated mice. (b, d, f, h, j, l, n, p, r, t) Higher magnification of areas indicated in (a, c, e, g, i, k, m, o, q, s). (u) Pathologic scores calculated based on five parameters: edema (E), hemorrhage (H), infiltrates (I), vacuolization (V), necrosis (N) of acinar cells. (t) Scores: total scores derived from the evaluation of five parameters. (v) Column graph of pathologic scores shown as mean ± s.d. (error bar). (w) Serum amylase levels. Black arrows indicate respective inflammatory changes. Scale bar: 50 μm. *$P < 0.05$. NS: no significance.

Normal diet (pancreas)

Low magnification | High magnification

CDE diet (pancreas)

Low magnification | High magnification

u Pathologic scores in CDE-diet acute pancreatitis

M. Strain	Treat	No. of Mice	E	H	I	V	N	Total Scores	Mean ± SD
JF1/Ms	N. Diet	5	2	1	0	0	0	3	0.6 ± 0.24
	CDE	5	2	2	0	3	0	7	1.4 ± 0.54
C57BL/6	N. Diet	5	1	0	0	0	0	1	0.2 ± 0.07
	CDE	5	3	0	0	2	0	5	1.0 ± 0.38
BALB/c	N. Diet	5	1	0	0	1	0	2	0.4 ± 0.57
	CDE	5	2	6	0	0	0	8	1.6 ± 0.32
CBA/J	N. Diet	5	2	0	0	0	0	2	0.4 ± 0.18
	CDE	5	3	3	0	1	5	12	2.4 ± 0.42
C3H/He	N. Diet	5	2	0	0	0	0	2	0.4 ± 0.2
	CDE	5	7	6	2	0	19	34	6.8 ± 1.40
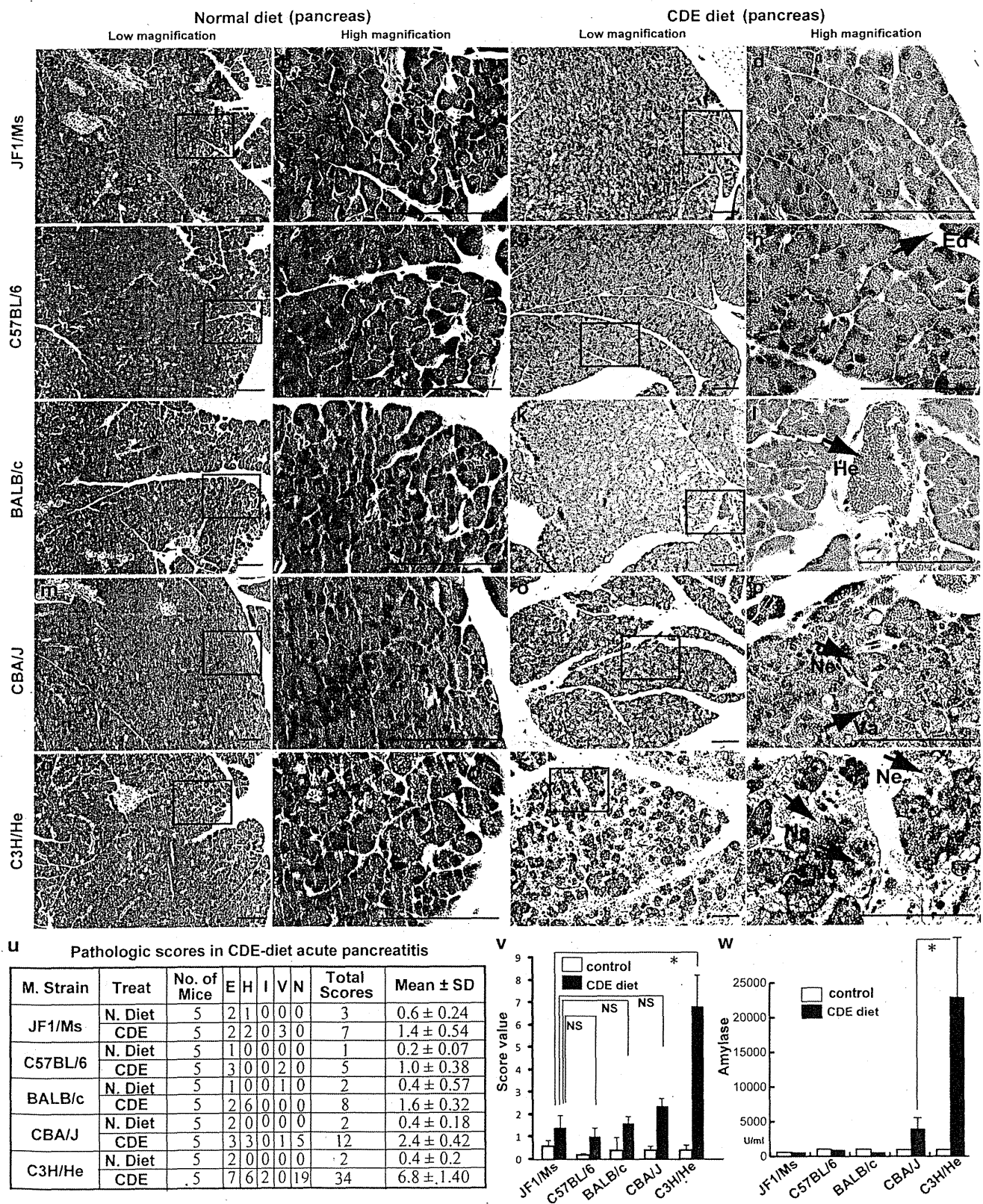
Figure 2 Histological changes, pathologic scores, and serum amylase levels in pancreas with and without CDE diet-induced acute pancreatitis.
(a, b, e, f, i, j, m, n, q, r) Saline-treated mice. (c, d, g, h, k, l, o, p, s, t) Cerulein-treated mice. (b, d, f, h, j, l, n, p, r, t) Higher magnification of areas indicated in (a, c, e, g, i, k, m, o, q, s). (u) Pathologic scores calculated based on five parameters: edema (E), hemorrhage (H), infiltrates (I), vacuolization (V), necrosis (N) of acinar cells. (v) Column graph of the pathologic scores shown as mean ± s.d. (error bar). (w) Serum amylase levels. Black arrows indicate respective inflammatory changes. Scale bar: 50 μm. *P<0.05. NS: no significance.